

Mesozoic and Cenozoic tectonic history of the central Chinese Tian Shan: Reactivated tectonic structures and active deformation

M. Jolivet, Stephane Dominguez, Julien Charreau, Yan Chen, Yongan Li, Qingchen Wang

▶ **To cite this version:**

M. Jolivet, Stephane Dominguez, Julien Charreau, Yan Chen, Yongan Li, et al.. Mesozoic and Cenozoic tectonic history of the central Chinese Tian Shan: Reactivated tectonic structures and active deformation. Tectonics, 2010, 29 (6), pp.TC6019. 10.1029/2010TC002712 . hal-00551323

HAL Id: hal-00551323
https://hal.science/hal-00551323

Submitted on 4 Jan 2011

HAL is a multi-disciplinary open access archive for the deposit and dissemination of scientific research documents, whether they are published or not. The documents may come from teaching and research institutions in France or abroad, or from public or private research centers.

L'archive ouverte pluridisciplinaire **HAL**, est destinée au dépôt et à la diffusion de documents scientifiques de niveau recherche, publiés ou non, émanant des établissements d'enseignement et de recherche français ou étrangers, des laboratoires publics ou privés.

Mesozoic and Cenozoic tectonic history of the central Chinese Tian Shan: Reactivated tectonic structures and active deformation

M. Jolivet,[1] S. Dominguez,[2] J. Charreau,[3] Y. Chen,[4] Yongan Li,[5] and Qingchen Wang[6]

Received 26 March 2010; revised 2 September 2010; accepted 20 September 2010; published 29 December 2010.

[1] The present-day topography of the Tian Shan range is considered to result from crustal shortening related to the ongoing India-Asia collision that started in the early Tertiary. In this study we report evidence for several episodes of localized tectonic activity which occurred prior to that major orogenic event. Apatite fission track analysis and (U-Th)/He dating on apatite and zircon indicate that inherited Paleozoic structures were reactivated in the late Paleozoic-early Mesozoic during a Cimmerian orogenic episode and also in the Late Cretaceous-Paleogene (around 65–60 Ma). These reactivations could have resulted from the accretion of the Kohistan-Dras arc or lithospheric extension in the Siberia-Mongolia zone. Activity resumed in the late Mesozoic prior to the major Tertiary orogenic phase. Finally, the ongoing deformation, which again reactivates inherited tectonic structures, tends to propagate inside the endoreic basins that were preserved in the range, leading to their progressive closure. This study demonstrates the importance of inherited structures in localizing the first increments of the deformation before it propagates into yet undeformed areas.
Citation: Jolivet, M., S. Dominguez, J. Charreau, Y. Chen, Y. Li, and Q. Wang (2010), Mesozoic and Cenozoic tectonic history of the central Chinese Tian Shan: Reactivated tectonic structures and active deformation, *Tectonics*, *29*, TC6019, doi:10.1029/2010TC002712.

1. Introduction

[2] The Tian Shan is a 2500 km long, up to 7400 m high, range extending through western China, Kazakhstan, and Kyrgyzstan (Figure 1). This range belongs to the larger Central Asian Orogenic Belt (CAOB) extending from the Urals to the Pacific across the East European, Siberian North China, and Tarim cratons [e.g., *Şengör et al.*, 1993; *Windley et al.*, 2007]. Several models have been proposed for the evolution of the CAOB. It is beyond the scope of this work to discuss these various models, and the reader interested in that discussion is referred to the synthesis of *Windley et al.* [2007]. The geochemical and tectonic data from the Tian Shan suggest multiple accretions of island arcs and Precambrian blocks rifted from Gondwana and/or Siberia [e.g., *Filippova et al.*, 2001; *Khain et al.*, 2003; *Buslov et al.*, 2004a].

[3] According to that model, the Tian Shan range has resulted from the amalgamation of a number of terranes during the Paleozoic [e.g., *Allen et al.*, 1993a; *Gao et al.*, 1998; *Laurent-Charvet*, 2001; *Zhou et al.*, 2001; *Glorie et al.*, 2010]. The Late Devonian to Early Carboniferous collision between the Tarim and Central Tian Shan blocks was followed by a Late Carboniferous-Early Permian collision between the Tarim-Central Tian Shan block and a series of island arcs currently exposed in the Northern Tian Shan [e.g., *Coleman*, 1989; *Wang et al.*, 1990; *Windley et al.*, 1990; *Allen et al.*, 1993a; *Carroll et al.*, 1995, 2001; *Charvet et al.*, 2009; *Biske and Seltmann*, 2010]. Compressive structures generated during these collision phases were then reworked by late Paleozoic strike-slip shear zones such as the Main Tian Shan Shear Zone (MTSZ) in central Tian Shan (Figure 1) [e.g., *Allen et al.*, 1991; *Che et al.*, 1994; *Laurent-Charvet et al.*, 2002, 2003]. This shearing phase, induced either by northward [*Chen et al.*, 1999; *Alexeiev et al.*, 2009] or northwestward [*Heubeck*, 2001] motion and clockwise rotation of the Tarim block, seems to have ended in Late Permian to Early Triassic, around 245 Ma [*Laurent-Charvet et al.*, 2003].

[4] The present-day topography of the range results from crustal shortening related to the ongoing India-Asia collision that started in early Tertiary time [e.g., *Tapponnier et al.*, 1986; *Avouac et al.*, 1993; *Najman and Garzanti*, 2000; *DeCelles et al.*, 2004; *Yin*, 2006, 2010]. Several intermontane basins, such as the Yili basin, the Turpan basin, and the Bayanbulak basin (Figure 1), are preserved within the interior of the Tian Shan range. The sedimentary series within these basins are typically composed of largely undeformed Tertiary detrital sediments deposited over faulted and folded Jurassic strata which lie unconformably over strongly deformed Paleozoic rocks [*Chen and Xu*, 1995; *Graham et al.*, 1994, *Zhou et al.*, 2001]. *Dumitru et al.* [2001] carried out a preliminary large-scale apatite fission track study of the Chinese Tian Shan along an approximately north-south transect across the entire range along the Duku road. The results showed highly heterogeneous cooling records across the range, with three main cooling episodes in latest Paleozoic, late Mesozoic, and late Cenozoic. From those data and in accordance with the overall topography of the range, the Tian Shan can be divided into a series of independent, generally east-west trending

[1]Laboratoire Géosciences Rennes, Université Rennes 1, UMR 6118 CNRS/INSU, Rennes, France.
[2]Laboratoire Géosciences Montpellier, Université Montpellier 2, UMR 5243 CNRS/INSU, Montpellier, France.
[3]Centre de Recherches Pétrographiques et Géochimiques, Vandoeuvre lès Nancy, France.
[4]Institut des Sciences de la Terre d'Orléans, Université d'Orléans, Orléans, France.
[5]Institute of Geology and Mineral Resources, Urumqi, China.
[6]State Key Laboratory of Lithospheric Evolution, Institute of Geology and Geophysics, Chinese Academy of Sciences, Beijing, China.

Copyright 2010 by the American Geophysical Union.
0278-7407/10/2010TC002712

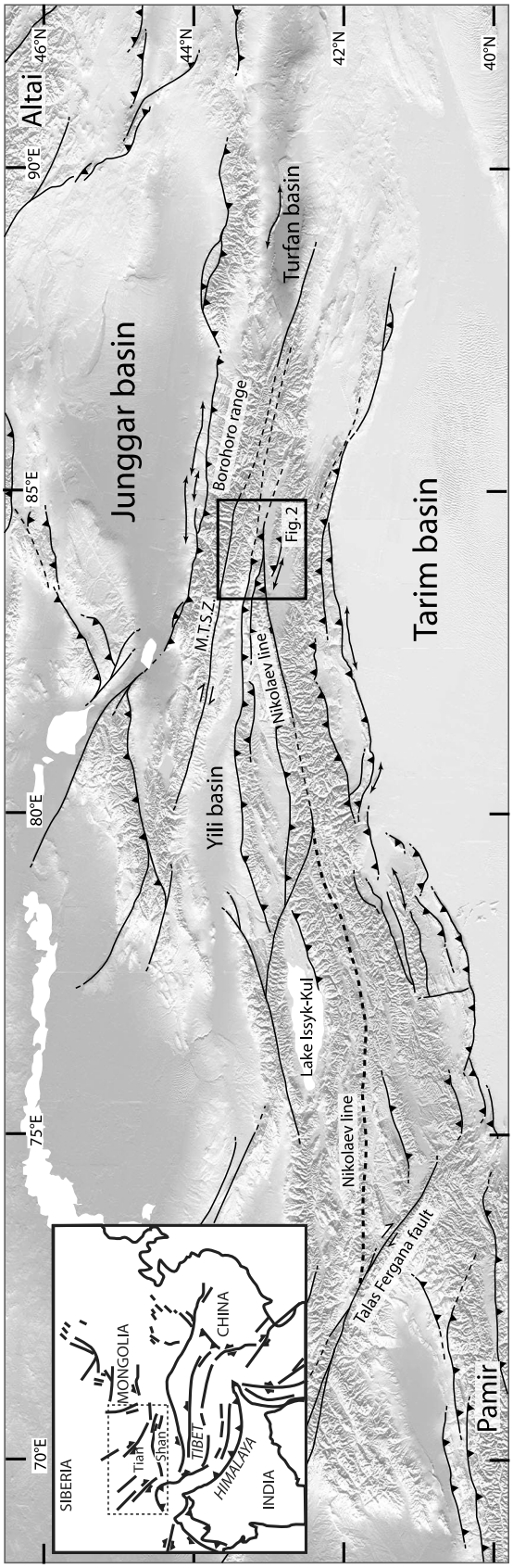


Figure 1. General topographic and tectonic map of the Tian Shan belt. Only the major tectonic structures are indicated. "M.T.S.Z." is the Main Tian Shan Shear Zone. To the west in Kyrgyzstan, the position of the Nikolaev line (bold dashed line) is drawn from *Burbank et al.* [1999]. The black square corresponds to the study area detailed in Figure 2.

subranges and intervening basins. Those individual units show quite variable differential exhumation [*Dumitru et al.*, 2001]. Paleozoic and Mesozoic apatite fission track ages indicate that little exhumation has occurred since early Mesozoic times over large areas within the Tian Shan range.

[5] Consequently, the intramontane Bayanbulak and Yili basins which have experienced only limited Tertiary deformation (Figure 2) must have retained the thermal history associated with the pre-Jurassic evolution of the range. We therefore targeted this area for a low-temperature thermochronology investigation (fission tracks and (U-Th)/He), aiming to constrain the Triassic to Present exhumation and topographic history of the range. We surveyed a transect perpendicular to the general E-W trend of the Tian Shan from the Borohoro range to the north, to the Bayanbulak basin in Central Tian Shan (Figures 1 and 2). We combined a tectonic study with apatite fission track analysis and apatite and zircon (U-Th)/He thermochronology to decipher the tectonic evolution of the range and intramontane basins.

2. Setting of the Yili-Bayanbulak Area

2.1. Geographic and Structural Geology Setting

[6] The central part of the Chinese Tian Shan comprises several intermontane basins separated by up to 4500–5000 m high ranges (Figure 2).

[7] To the north, the Borohoro range separates the Yili basin from the North Tian Shan piedmont in the Junggar basin. The basement of the range is mainly composed of a Devonian to Carboniferous magmatic arc intruded by Devonian granitoids [e.g., *Zhou et al.*, 2001]. On the southern and northern sides of the range, the basement is capped by Permian sediments, mainly carbonates. The Borohoro range is itself separated in two compartments by the small, elongated Hexilagen basin in which Early Jurassic coal series are exposed (Figure 2). These series are folded, generally tilted to the south, and unconformably overlaid by horizontal or slightly tilted to the south Tertiary (Eocene) clastic sediments [*Xinjiang Bureau of Geology and Mineral Resources* (*XBGMR*), 1973] (Figure 3).

[8] South of the Borohoro range, the Yili basin is filled with Eocene to Quaternary clastic sediments. There is no outcrop evidence of Mesozoic series at least in the eastern part of the basin.

[9] To the south, the Yili basin is separated from the larger Bayanbulak basin by the W-E trending Narat range (Figure 2). The basement of this range is composed of Proterozoic gneisses [*Gao et al.*, 1998] dated at 1.3 ± 0.2 Ga (U/Pb on zircon) and 1.1 ± 0.12 Ga (Sm/Nd on whole rock) [*Wang et al.*, 1994]. This Proterozoic basement is intruded by numerous Late Ordovician granite plutons [*Ma et al.*, 1993; *Che et al.*, 1994; *Zhou et al.*, 2001]. In the central part of the range, Carboniferous volcanic series (basalts, tuffs, pillow lavas, and associated volcanic-clastic sediments) are thrust southward over Silurian marbles and volcanics (andesitic tuffs and volcanic breccia). The whole package overlies the gneissic Proterozoic basement. Immediately north of the Laerdun pass along the road that crosses the Narat range (Figure 2), peridotite and serpentinite fragments are trapped within the basement gneisses, possibly indicating the remnants of a suture zone [*Laurent-Charvet*, 2001]. Numerous strike-slip mylonitic zones have been described in the Narat range, running about E-W parallel to the actual topography [*Laurent-Charvet*, 2001]. South of the Laerdun pass, the Silurian volcanites are separated from the Proterozoic basement by a major shear zone [*Laurent-Charvet*, 2001]. Following *Dumitru et al.* [2001], we interpret this wide fault zone as representing the eastward prolongation of the Nikolaev line (Figure 1) [e.g., *Dumitru et al.*, 2001]. This tectonic lineament corresponds to a major fault zone in the Kyrgyz Tian Shan [*Burtman*, 1975]. The northern zone was deformed during early Paleozoic times while the southern zone was deformed during late Paleozoic times.

[10] Inside the Narat range, the small endoreic Narat basin (Figure 2) is also filled with Neogene to Quaternary sediments. As in the Yili basin, the geological map [*XBGMR*, 1969, 1971] reports no evidence of Mesozoic sediments. Our own field investigation did not reveal any Mesozoic sediments, but we cannot exclude that there might be some below the Neogene to Quaternary cover.

[11] South of the Narat range, the Bayanbulak basin is a wide endoreic sedimentary basin filled by large river fans (Figure 2). The base level of the basin is at an altitude of about 2400 m, while the fans reach altitudes of about 3000 m all around the basin. As in the Hexilagen basin, coal-bearing Jurassic sediments are well described in the northern part of the basin. The geological map [*XBGMR*, 1969, 1971] does not show any Cretaceous or Paleocene sediments. However, a 1.5 km long section exposed in a deeply incised canyon northeast of Bayanbulak city revealed that such series may exist in the basin (Figures 4a and 4b). The Jurassic series are composed of 10 cm to several meters thick gray sandstone to conglomerate beds, intercalated with shale and coal. This series is overlain conformably by a series of concordant red, fine to medium grained sandstones. The transition between the two units is marked by 2–3 m thick conglomerates cemented by carbonates. By comparison with the sections described in the northern and southern piedmonts of the Tian Shan [e.g., *Hendrix et al.*, 1992; *Sobel*, 1999], we interpret the red beds as Lower Cretaceous series. Further up in the series, the exposure is not complete and further investigation will be needed. However, it is probable that sedimentation in these intramontane basins continued during the Cretaceous and possibly until the early Tertiary.

[12] East of Bayanbulak city, the >4000 m high Erbin Shan range is formed by a Devonian granite pluton dated at 378 Ma (U/Pb on zircon [*Hu et al.*, 1986; *Zhou et al.*, 2001]) associated with Devonian and Carboniferous volcanic breccia and conglomerates.

[13] Finally, the Bayanbulak basin is bounded to the south by the South Tian Shan range composed of Ordovician, Silurian, and Devonian flysch and marbles, intruded by a few late Paleozoic granites [*Gao et al.*, 1998].

2.2. Active Tectonic Setting

[14] We assessed active tectonic activity in the study area based on satellite images and our field observations. We looked for geomorphic evidence of active tectonics (deformed fluvial or fan terraces, perturbation of the drainage

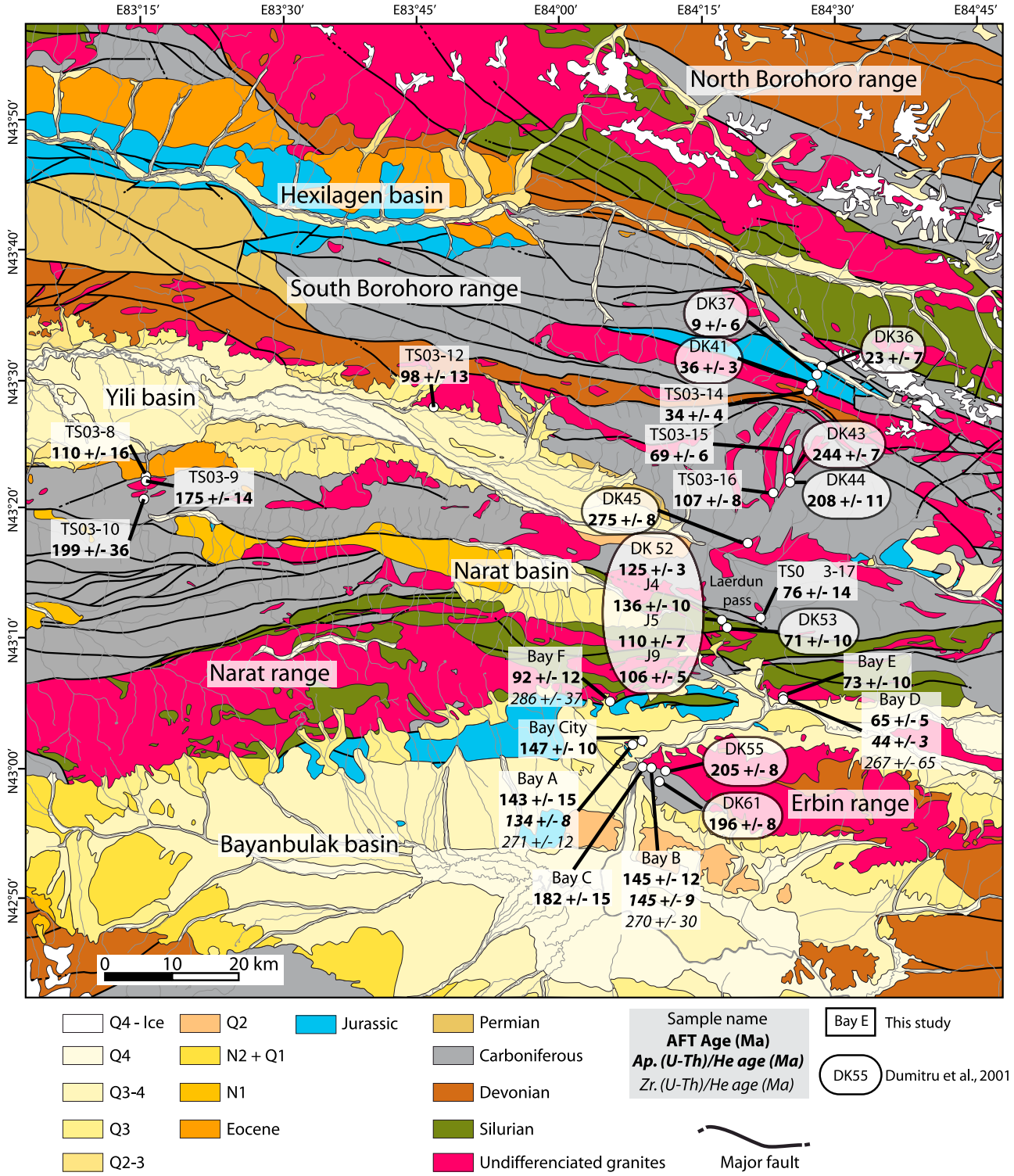


Figure 2. Geological map of the study area (modified after the 1:200,000 geological maps [*XBGMR*, 1969, 1971, 1973] using satellite images and field observations) showing the main tectonic structures. For clarity, active faults are represented in detail on Figure 5. Samples from this study and from *Dumitru et al.* [2001] are indicated with the corresponding apatite fission track and zircon and apatite (U-Th)/He ages. See Tables 1 and 2 for detailed data.

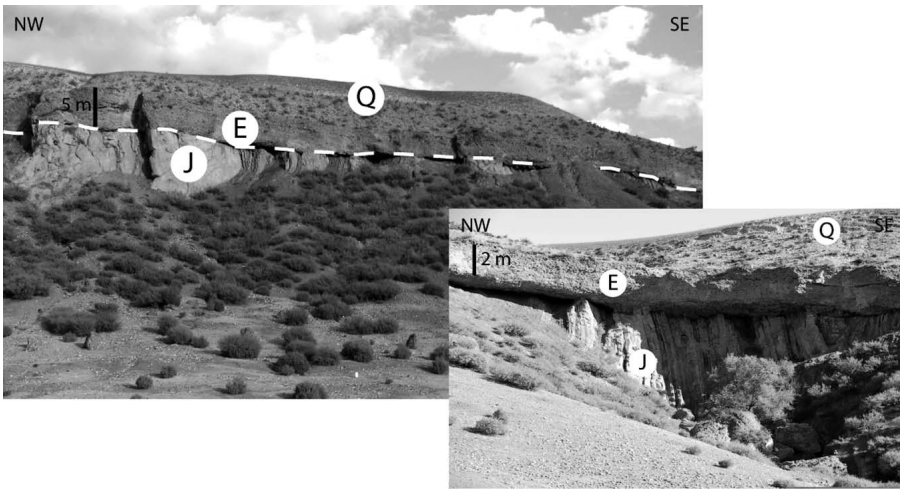


Figure 3. Pictures of the unconformity (white dashed line) between the Jurassic and Tertiary sediments within the Yili basin. The picture was taken west of the study area where the Yili and Hexilagen basins meet. The vertical scale is indicated. The Jurassic (J) coal-bearing conglomerates and sandstones have been deformed prior to the deposition of the Eocene (E) sandstones which are themselves covered by the Quaternary (Q) deposits. No evidence of Cretaceous sediments has been found in the Yili basin, and only localized Cretaceous deposits have been recognized on the northern edge of the Bayanbulak basin (see Figure 4 and text for discussion).

network). The main findings of those investigations are summarized below. We have not indentified any clear active faults in the Hexilagen basin. However, the deeply incised valley that continues the basin toward the east and separates the North Borohoro range from the South Borohoro range is bounded by a south dipping thrust fault (Figure 5).

[15] Active faulting clearly affects the northern side of the Narat range (Figure 5). Morphological and structural evidence suggests that south dipping reverse faults control the southern boundary of the Yili basin where Quaternary sediments, overlaid by thick loess deposits, are clearly uplifted and folded (Figure 6). Within the small Narat basin, south dipping thrust faults cut and offset the Pliocene-Quaternary cover composed of alluvial and colluvial deposits shed from the nearby Narat range.

[16] South of the Narat range, several reverse fault scarps and associated E-W trending structural ridges affect the smooth surface morphology of the Bayanbulak basin (Figure 4). Active faults appear to be mainly concentrated in the northern part of the basin, around the latitude of Bayanbulak city (43°N). They follow the southern slope break of the Narat range for more than 50 km to the west of the longitude of the Laerdun pass (84°20′E) (Figure 5). Further to the east Quaternary deposits are deformed by faults and folds which are observed over a distance of more than 50 km along the range [*Fu et al.*, 2003]. The fault zone bounding the northern side of the Bayanbulak basin and its eastern prolongation can thus be considered as a major regional active tectonic contact. It can be noticed that this fault zone trends parallel to the mapped trace of the Nikolaev line (Figures 1 and 5).

[17] The general structure and the pattern of active deformation suggest that the faults affecting the North Bayanbulak basin and those located on the northern side of the Narat range join at depth into a single major crustal-scale thrust fault system (Figure 5). The E-W trending Narat range could be, then, interpreted as a major pop-up structure, bounded by south and north dipping thrust faults. Because the location of these faults and their orientation are coherent with the assumed trace of the Nikolaev line in this region (Figure 5), we propose that they correspond to the reactivation of this main structure in response to Cenozoic compression. Such a reactivation of Proterozoic and Paleozoic fault zones has already been demonstrated in the Kyrgyz Tian Shan further west [e.g., *Buslov et al.*, 2004b, 2007].

3. Low-Temperature Thermochronology

[18] The locations of the samples used in this study are reported in Figure 2, and details are provided in Table 1 (precise coordinates, altitude, and lithology), Table 2 (fission track analysis results), and Table 3 ((U-Th)/He results).

3.1. Apatite Fission Track Analysis

[19] The apatite samples were mounted on glass slides using epoxy glue and polished. Samples were etched in 6.5% HNO_3 (1.6 M) for 45 s at 20°C to reveal the spontaneous fission tracks [*Seward et al.*, 2000], before being irradiated with a neutron fluence rate of 1.0×10^{16} neutrons/cm^2 (ANSTO, Lucas Height, Australia). The micas used as external detector were etched in 40% HF for 40 min at 20°C in order to reveal the induced fission tracks. The ages were calculated following the method recommended by the Fission Track Working Group of the International Union of Geological Sciences Subcommission on Geochronology [*Hurford*, 1990] using the zeta calibration method [*Hurford and Green*, 1983]. CN5 glass was used as a dosimeter. Ages were calculated using an overall weighted mean zeta value of 342 ± 20 yr cm^2 (MJ), obtained on both Durango

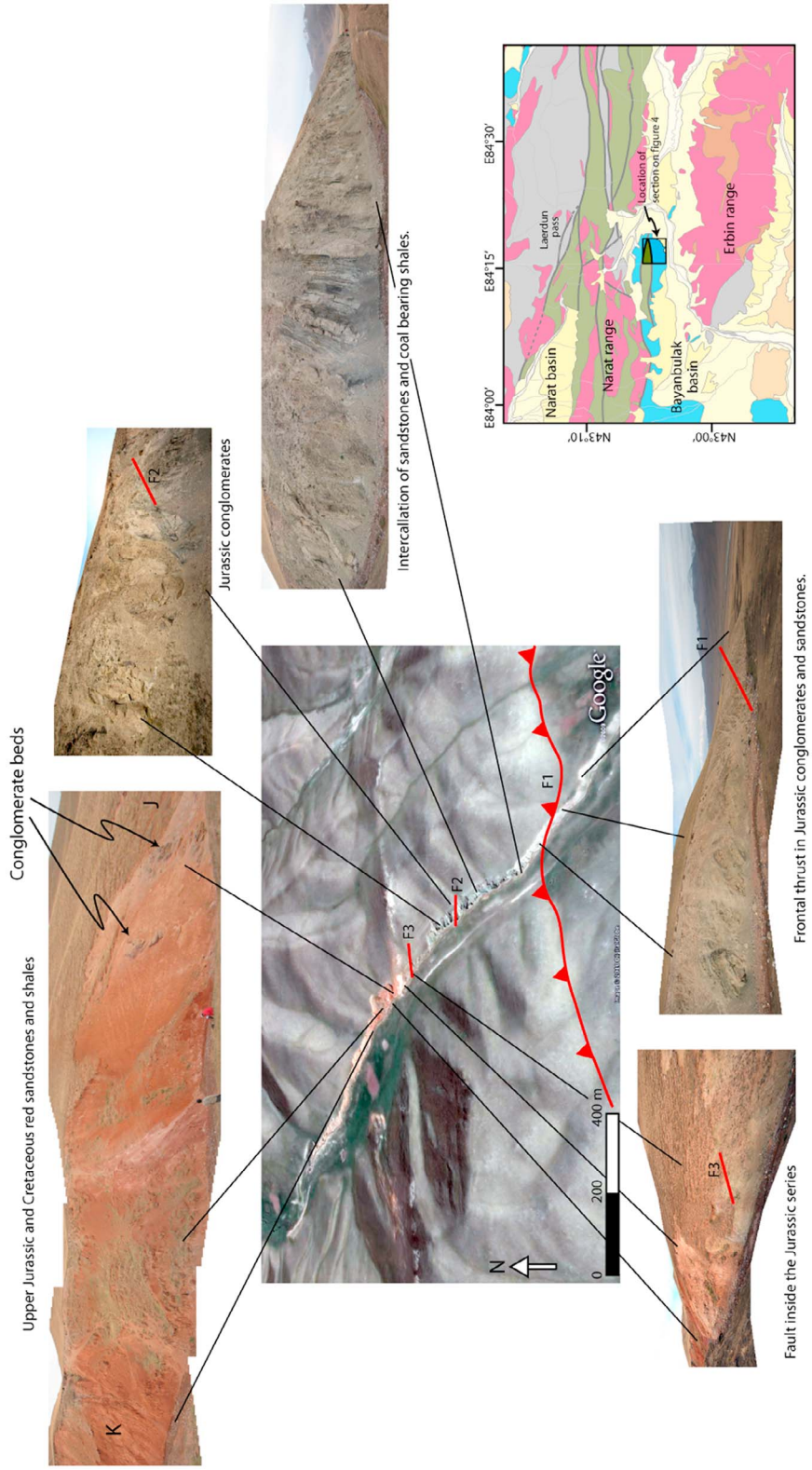


Figure 4a. Pictures of the Jurassic (J) and Cretaceous (K) series exposed in the small canyon north of the Bayanbulak basin (see text for lithological description of the series). The general satellite view of the outcrop is from Google Earth. The small geological map showing the location of the outcrops is from Figure 2. The section is cut by several north verging thrust faults, but only the frontal one (F1) shows evidence of activity during the Quaternary. Faults F2 and F3 are cutting through the stratigraphy and are locally associated with breccia. However, it was not possible to see any displacement in the thin Quaternary soil deposits on the surface of the outcrop. This deformation is consistent with the uplift of the Narat range immediately to the north.

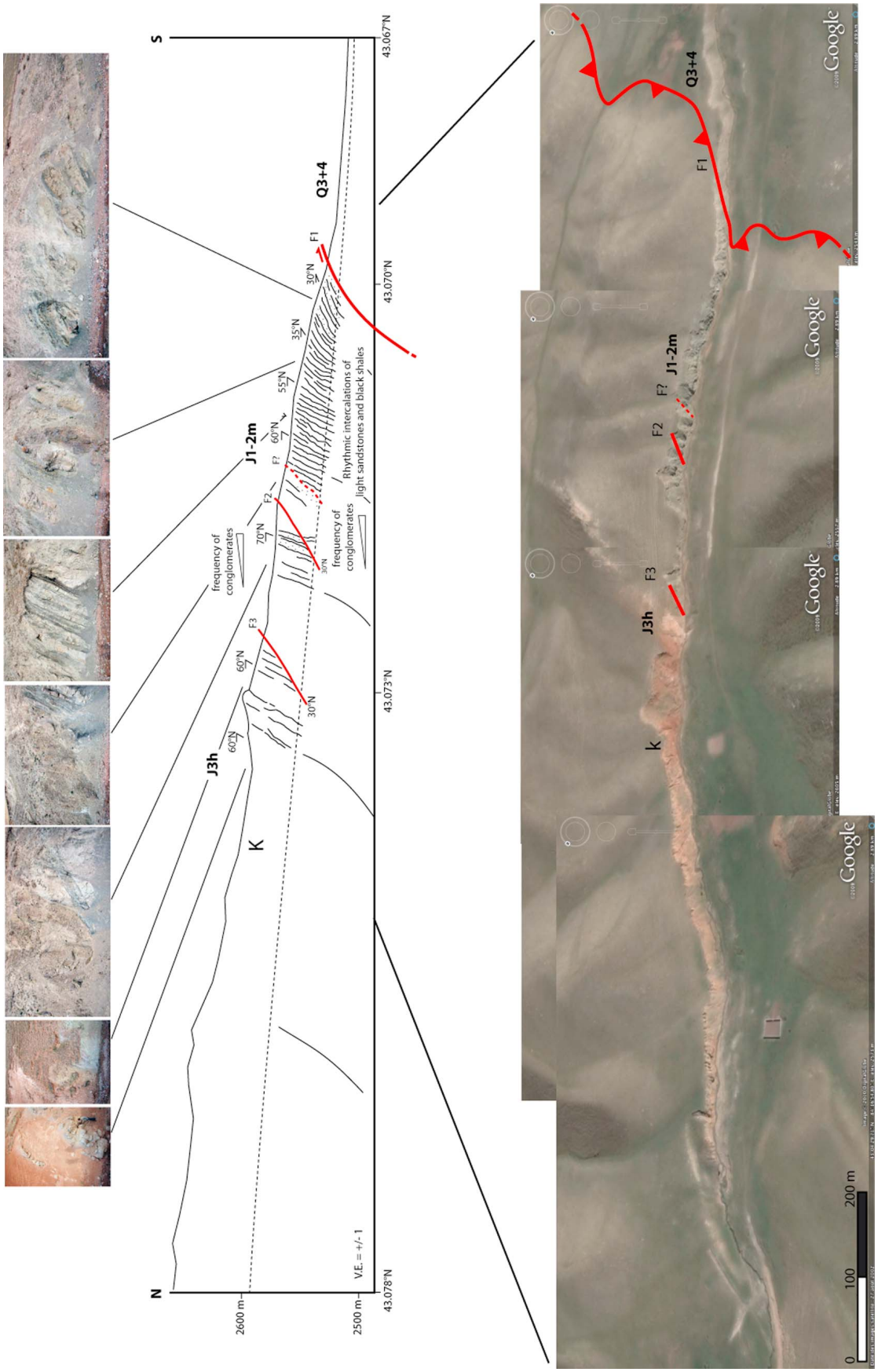


Figure 4b. Structural cross section along the canyon. The stratigraphic ages for the Jurassic (J_{3h} and J_{1-2m}) and Quaternary (Q_{3+4}) are from the 1:200,000 geological map [*XBGMR*, 1969]. The Cretaceous sediments are marked "K," because we do not have precise age indication. The lower panel shows a satellite view of the section (from Google Earth).

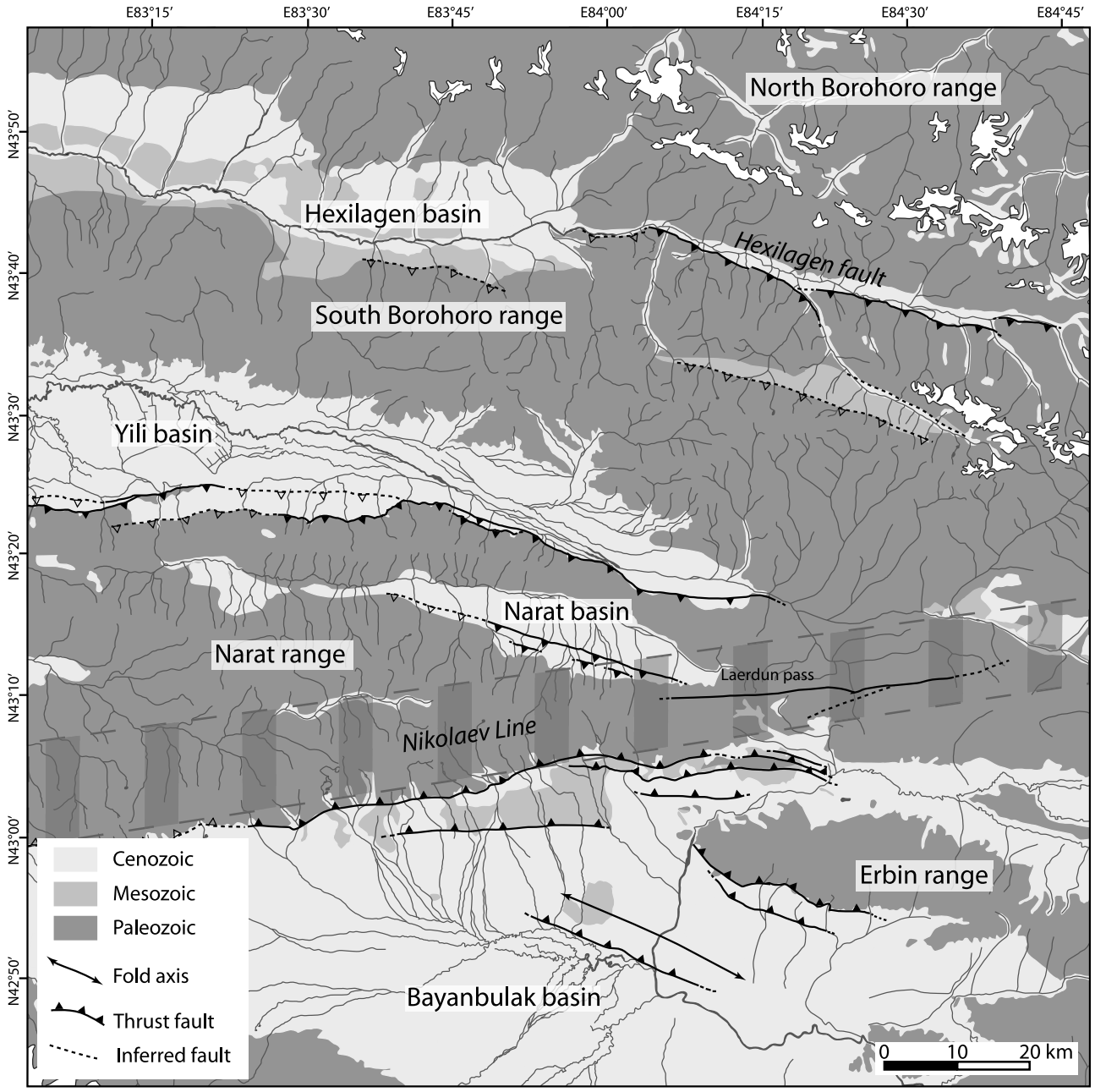


Figure 5. Simplified geological map of the study area (modified after the 1:200,000 geological maps [*XBGMR*, 1969, 1971, 1973] using satellite images and field observations) showing the active faults recognized in the field or on satellite images. Inferred active faults are mostly drawn from satellite images, while no clear evidences could be found in the field. Note that both sides of the Narat range are affected by active deformation, while only a few faults are observed within the Borohoro range. Also note the dissymmetric tectonic structure of the Yili and Hexilagen basins. The striped zone indicates the suspected location of the inherited Nikolaev line tectonic structure.

[*McDowell et al.*, 2005] and Mount Dromedary apatite standards [*Green*, 1985; *Tagami*, 1987]. Fission tracks were counted on a Zeiss microscope, using a magnification of 1250 under dry objectives. Data are reported in Table 2.

[20] All ages from this study are central ages except for sample Bay A, which has $P(\chi^2) < 5\%$ and for which the pooled age has been considered more representative although equal to the central age within the error margin (see *Galbraith and Laslett* [1993] or *Galbraith* [2005] for details on the calculation of both ages). *Dumitru et al.* [2001] only reported central ages even when the corresponding $P(\chi^2)$ value was less than 5%. When this is the case, the central and pooled ages are slightly different but the difference generally falls within the error margin and does not influence the discussion



Figure 6. Picture of the deformation affecting the Tertiary and Quaternary sediments inside the Yili basin, immediately north of the Narat range. The northernmost basement thrust controlling the exhumation of the Narat range is shown (solid line), as is the inferred position of the hidden frontal thrust inside the sediments of the Yili basin (dotted line). The 100–200 m high hills are formed by folding of the sediments in front of the basement thrust.

of the data. Errors on ages from this study are quoted at $\pm 2\sigma$, while ages from *Dumitru et al.* [2001] are quoted at $\pm 1\sigma$. In some of the samples (either from *Dumitru et al.* [2001] or from this study), the number of analyzed crystals is lower than the usually targeted 20. We cannot discuss the reasons for this in the work of *Dumitru et al.* [2001], but in our samples the poor quality of the apatite crystals, and especially the occurrence of tiny zircon inclusions that generate "alien" fission tracks, prevented us from reaching the number of 20 crystals for analysis. In order to get the best possible result, we preferred to analyze a small number of good crystals rather than a larger number of possibly flawed ones.

[21] Thermal history modeling was done using the HeFTy software [*Ketcham*, 2005] with the annealing model of

Table 1. Geographic Position, Altitude, and Lithology of the Samples Used in This Study[a]

Sample	Latitude	Longitude	Altitude	Lithology
			This Study	
Bay A	43°2.126′N	084°8.526′E	2505	Granite probably intrusive in Carboniferous (C_1) series
Bay B	43°0.425′N	084°8.692′E	2457	Granite (378 Ma U-Pb age[b]) covered by Carboniferous (C_1) breccia
Bay C	43°0.538′N	084°8.249′E	2437	Granite (378 Ma U-Pb age[b]) covered by Carboniferous (C_1) breccia
Bay D	43°5.458′N	084°22.829′E	2583	Tonalite intruded within the Silurian (S_3) metamorphic series
Bay E	43°5.373′N	084°22.818′E	2550	Tonalite intruded within the Silurian (S_3) metamorphic series
Bay F	43°4.946′N	084°4.608′E	2766	Granite intruded within the Silurian (S_3) metamorphic series
Bay City	43°1.690′N	084°8.338′E	2500	Granite probably intrusive in Carboniferous (C_1) series
TS-03-8	43°21.634′N	083°15.076′E	982	Andesitic dyke within the carboniferous (C_1) magmatic series
TS-03-9	43°21.125′N	083°14.764′E	1004	Granodiorite intruded within the Carboniferous (C_1) series
TS-03-10	43°21.679′N	083°15.076′E	993	Granite intruded within the Carboniferous (C_1) series
TS-03-12	43°27.887′N	083°44.382′E	1038	Granite intruded within the Devonian (D_2) series
TS-03-14	43°28.299′N	084°26.656′E	3361	Granite intruded within the Carboniferous (C_1) series
TS-03-15	43°24.893′N	084°23.086′E	2506	Deep red granite intruded within the Carboniferous (C_2) series
TS-03-16	43°21.935′N	084°21.678′E	1900	Granite intruded within the Carboniferous (C_2) series
TS-03-17	43°11.630′N	084°20.294′E	2238	Deep red granite intruded within the Carboniferous (C_1) series
			From Dumitru et al. [2001]	
DK36	43°30.6′N	084°27.4′E	3010	Silurian (S_{1-2}) metamorphic rock
DK37	43°29.5′N	084°27.1′E	3280	Granite intruded within the Silurian (S_{1-2}) metamorphic series
DK41	43°28.6′N	084°27.0′E	3360	Granite intruded within the Silurian (S_{1-2}) metamorphic series
DK43	43°23.2′N	084°23.2′E	2400	Granite intruded within the Carboniferous (C_2) series
DK44	43°23.0′N	084°23.2′E	2280	Granite intruded within the Carboniferous (C_2) series
DK45	43°17.4′N	084°18.9′E	1760	Igneous rock of unknown affinity
DK52	43°11.3′N	084°17.3′E	2560	Silurian metamorphic rock
DK53	43°10.9′N	084°17.6′E	2640	Granite (378 Ma U-Pb age[b]) covered by Carboniferous (C_1) conglomerates
DK55	43°00.1′N	084°09.8′E	2710	Lower Carboniferous (C_1) conglomerates
DK61	42°59.9′N	084°08.9′E	2660	Silurian metamorphic rock
J4	43°11.3′N	084°17.3′E	2560	Silurian metamorphic rock with biotite $^{40}Ar/^{39}Ar$ plateau age[c] of 286 ± 2.6 Ma
J5	43°11.3′N	084°17.3′E	2560	Silurian metamorphic rock
J9	43°11.1′N	084°17.4′E	2600	Silurian metamorphic rock

[a]The ages of the series are from the Chinese geological maps [*XBGMR*, 1969, 1971, 1973].
[b]Precise ages are from *Hu et al.* [1986] and *Zhou et al.* [2001].
[c]Precise age is from *Zhou et al.* [2001].

Table 2. Fission Track Analysis[a]

Sample	Number of Grains	$\rho_d \times 10^4$ (cm^{-2})	$\rho_s \times 10^4$ (cm^{-2})	$\rho_i \times 10^4$ (cm^{-2})	[U] (ppm)	$P(\chi^2)$ (%)	Measured D_{par} (μm)	Corrected D_{par} (μm)	Mean Track Length (μm) ($\pm1\sigma$)	SD (μm)	FT age (Ma)
This Study											
Bay A	20	104.6 (6547)	108.03 (444)	122.14 (502)	14	2	2.0	1.7	12.0 ± 0.2 (100)	1.8	143.3 ± 14.6
Bay B	18	113.6 (6331)	73.03 (444)	89.97 (547)	11	82	2.6	2.1	12.7 ± 0.2 (100)	1.7	145.0 ± 11.8
Bay C	19	113.6 (6547)	81.47 (431)	80.15 (424)	8	94	2.0	1.7	12.4 ± 0.1 (101)	1.5	182.0 ± 15.4
Bay D	20	95.53 (6547)	104.35 (480)	242.17 (1114)	30	36	3.7	3.1	14.0 ± 0.1 (100)	1.5	65.1 ± 4.8
Bay E	4	110.9 (6331)	134.92 (85)	325.4 (205)	36	81	3.8	3.1	-	-	72.7 ± 10.1
Bay F	13	97.42 (6331)	50.24 (106)	84.36 (178)	10	98	1.6	1.3	12.1 ± 0.2 (10)	1.9	91.6 ± 12.1
Bay City	19	100.1 (6331)	133.95 (801)	143.81 (860)	16	35	2.2	1.8	12.1 ± 0.2 (103)	2.0	147.2 ± 10.5
TS-03-8	13	125.6 (9392)	39.9 (81)	71.92 (146)	8	81	2.1	1.7	13.6 ± 0.1 (104)	1.4	110.4 ± 16.2
TS-03-9	17	121.5 (9392)	67.55 (433)	73.95 (474)	8	99	1.9	1.6	13.5 ± 0.1 (100)	1.2	175.0 ± 14.5
TS-03-10	10	115.4 (9392)	37.04 (70)	33.86 (64)	3	99	2.0	1.7	-	-	198.7 ± 35.7
TS-03-12	19	109.2 (9392)	53.89 (97)	95.0 (171)	11	97	2.0	1.7	13.2 ± 0.2 (101)	1.8	98.3 ± 13.4
TS-03-14	14	125.3 (6512)	53.5 (84)	315.29 (495)	13	88	2.2	1.8	-	-	34.4 ± 4.4
TS-03-15	20	120.1 (6512)	48.55 (217)	135.79 (607)	13	71	1.9	1.6	12.7 ± 0.2 (75)	2.2	69.2 ± 6.5
TS-03-16	20	115.0 (6512)	76.28 (643)	131.08 (1105)	14	12	2.3	1.9	12.2 ± 0.2 (100)	2.0	107.3 ± 8.3
TS-03-17	9	109.8 (6512)	47.96 (47)	111.22 (109)	13	56	2.6	2.1	11.8 ± 0.2 (27)	2.1	76.3 ± 13.9
From Dumitru et al. [2001]											
DK36	15	186.7 (5073)	6.86 (12)	108.6 (190)	-	61	-	-	-	-	22.7 ± 6.8
DK37	5	186.7 (5073)	2.34 (2)	92.35 (79)	-	8	-	-	-	-	9.1 ± 6.5
DK41	9	188.8 (5073)	99.19 (162)	1008.0 (1646)	-	38	-	-	13.6 ± 0.2 (37)	1.43	35.8 ± 3.0
DK43	24	188.8 (5073)	212.5 (2467)	310.7 (3606)	-	43	-	-	13.3 ± 0.2 (101)	1.73	244.5 ± 7.3
DK44	11	190.9 (5073)	214.2 (610)	372.5 (1061)	-	85	-	-	12.5 ± 0.2 (102)	2.00	208.3 ± 11.0
DK45	25	190.9 (5073)	142.1 (2835)	186.0 (3710)	-	84	-	-	13.5 ± 0.1 (105)	1.42	275.4 ± 7.9
DK52	28	170.3 (4808)	37.95 (839)	98.57 (2179)	-	75	-	-	13.1 ± 0.1 (100)	1.21	125.3 ± 5.4
DK53	5	168.3 (4808)	38.58 (57)	176.0 (260)	-	60	-	-	12.9 ± 0.2 (33)	1.39	70.8 ± 10.0
DK55	25	166.3 (4808)	154.4 (2108)	238.0 (3248)	-	1	-	-	12.4 ± 0.1 (150)	1.42	204.9 ± 8.4
DK61	21	193.0 (5073)	106.6 (1128)	198.9 (2104)	-	34	-	-	12.4 ± 0.5 (23)	2.17	196.6 ± 7.8
J4	11	170.3 (4808)	156.5 (566)	375.0 (1356)	-	3	-	-	12.3 ± 0.1 (151)	1.64	135.7 ± 9.7
J5	14	173.3 (4808)	38.79 (399)	116.6 (1199)	-	14	-	-	13.0 ± 0.1 (150)	1.52	110.3 ± 6.6
J9	10	173.3 (4808)	145.0 (719)	453.2 (2247)	-	44	-	-	12.2 ± 0.1 (150)	1.65	106.1 ± 4.8

[a]The parameter ρ_d is the density of induced fission track density (per cm^2) that would be obtained in each individual sample if its U concentration was equal to the U concentration of the CN5 glass dosimeter. Numbers in parentheses are total numbers of tracks counted; ρ_s and ρ_i represent the sample spontaneous and induced track densities per cm^2. Numbers in parentheses are total numbers of tracks counted. [U] is the calculated uranium density (in ppm). $P(\chi^2)$ is the probability in % of χ^2 for ν degrees of freedom (where ν = number of crystals −1). Measured D_{par} is the measured mean diameter (in μm) of the etched trace of the intersection of a fission track with the surface of the analyzed apatite crystal, measured parallel to the *c* axis. The slow etch protocol used in this study is not directly compatible with the use of the D_{par} parameter for statistical modeling of the fission data. For that reason the measured D_{par} value has been corrected (corrected D_{par}) using the equation of *Sobel and Seward* [2010]. See text for discussion on that issue. Mean track length is the measured mean fission track length in μm. Track length measurements were performed on horizontal confined fission tracks in crystal sections parallel to the *c* crystallographic axis. Length values are *c* axis projected values. Error is $\pm1\sigma$. Numbers in parentheses are total numbers of tracks measured. FT age is the apatite fission track age in Ma. When $P(\chi^2) < 5\%$, the considered FT age is the pooled age. When $P(\chi^2) > 5\%$, the considered FT age is the central age. Ages have been calculated using the TRACKKEY software [*Dunkl*, 2002]. Error is $\pm2\sigma$ for data analyzed in this study and $\pm1\sigma$ for data from *Dumitru et al.* [2001].

Ketcham et al. [1999] that takes into account the D_{par} parameter (see below). Variation in fission track annealing (and thus in apparent fission track age and mean track lengths) is correlated with the apatite cell parameters and thus is linked to crystallographic structure. For example, fission tracks oriented parallel to the crystallographic *c* axis have a higher mean etchable length than fission tracks oriented perpendicular to this axis [e.g., *Green and Durrani*, 1978; *Green*, 1981; *Donelick*, 1991]. For that reason, as a general standard, only crystal sections that are parallel to the *c* axis will be analyzed (for age determination and for track length measurements). Fission tracks are distributed in all directions within the apatite crystals, but to provide an accurate length measurement, only horizontal tracks, parallel to the sample's surface and confined in the crystal (i.e., do not cross the surface and are thus not partially cut), were measured (track length measurements are *c* axis projected values). Measurements were performed under reflected light at 1250X magnification (dry) and using a drawing tube coupled to a digitizing tablet and the FTStage software [*Dumitru*, 1993]. The track length distribution histograms are presented in Figure 7. The apatite chemical composition, and especially the Cl and F contents, also controls the annealing properties of the fission tracks [*Donelick*, 1993; *Burtner et al.*, 1994; *Barbarand et al.*, 2003]. For example, an increase in Cl content will slow the annealing process and increase the apparent fission track age and mean track length and diameter relative to a more F rich apatite. Variations in the fission track sensitivity to annealing can thus be deduced from variations of the fission track diameter. The D_{par} used as an input parameter in the HeFTy model corresponds to the diameter of the etched trace of the intersection of a fission track with the surface of the analyzed apatite crystal measured parallel to the *c* axis. As indicated above, due to anisotropic behavior of the fission tracks the D_{par} is only measured on sections parallel to the *c* axis. Measurements were performed using the same apparatus as for the fission track lengths but with a magnification of 2000X. Each D_{par} value reported in Table 2

Table 3. (U-Th)/He Analytical Protocol and Results[a]

Sample	Location	Altitude (m)	mass (μg)	F_T	He (nmol/g)	U (ppm)	Th (ppm)	Age (Ma)	Corrected Age (Ma)
				Apatite Samples					
Bay A (a)	43°2.126′N/084°8.526′E	2505	9.52	0.80	6.69	8.43	16.61	99.1	123.5
Bay A (b)	-	-	3.77	0.74	8.02	9.11	17.15	111.3	150.3
Bay A (c)	-	-	3.47	0.73	6.87	7.98	14.91	109.1	149.6
Bay A (d)	-	-	3.08	0.72	7.21	12.26	18.31	79.6	110.9
Bay B (a)	43°0.425′N/084°8.692′E	2457	6.31	0.77	7.26	6.95	13.67	130.1	168.9
Bay B (b)	-	-	4.87	0.74	13.63	16.50	47.28	90.3	121.2
Bay D (a)	43°5.458′N/084°22.829′E	2583	13.20	0.82	6.37	24.16	49.75	32.6	39.9
Bay D (b)	-	-	9.52	0.80	9.31	23.15	55.61	47.2	58.9
Bay D (c)	-	-	4.63	0.74	6.97	26.68	58.41	31.7	42.6
Bay D (d)	-	-	2.79	0.70	5.93	35.26	41.01	24.2	34.5
				Zircon Samples					
Bay A (a)	43°2.126′N/084°8.526′E	2505	21.32	0.8	1010.744	806.1654	335.7868	205.8	259.2
Bay A (b)	-	-	37.004	0.8	754.58387	511.1031	259.7278	236.9	284.6
Bay A (c)	-	-	14.012	0.8	223.59026	506.2227	189.2726	74.2	96.3
Bay B (a)	43°0.425′N/084°8.692′E	2457	48.808	0.8	210.93816	160.0113	110.7319	204.5	241.2
Bay B (b)	-	-	44.59	0.8	341.86493	209.7714	122.1288	257.1	303.2
Bay B (c)	-	-	24.561	0.8	245.19605	192.4399	121.4662	200.2	246.2
Bay B (d)	-	-	18.839	0.8	341.30066	231.437	153.215	229.6	288.8
Bay D (a)	43°5.458′N/E084°22.829′E	2583	87.039	0.9	430.86154	126.8567	100.2238	500.2	567.2
Bay D (b)	-	-	260.148	0.9	296.60277	167.5809	66.96836	288.8	316.0
Bay D (c)	-	-	107.46	0.9	817.09018	481.6908	327.0121	262.3	299.0
Bay D (d)	-	-	32.957	0.8	733.43529	737.312	588.5514	152.0	186.1
Bay F (a)	43°4.946′N/084°4.608′E	2766	18.259	0.8	361.40126	234.944	392.5734	199.8	252.9
Bay F (b)	-	-	9.422	0.7	217.04309	167.3753	126.0412	198.9	270.1
Bay F (c)	-	-	29.426	0.8	214.68597	121.0865	166.7366	241.3	292.4
Bay F (d)	-	-	27.247	0.8	259.85167	138.7868	138.3415	272.1	327.7

[a]Samples were analyzed at the Noble Gas Laboratory at the California Institute of Technology. Crystals were selected by hand picking and microscopic analysis on the basis of morphology, size, and absence of visible defects and inclusions (especially for apatite). The dimensions of the grains were measured in order to determine the necessary α-ejection correction (F_T) [*Farley et al.*, 1996]. In order to prevent a wide spread in the F_T values, the crystals analyzed in this study were of approximately the same size in most of the aliquots (Table 3). Individual aliquots were composed of one crystal for apatite and two crystals for zircon. Two to four aliquots were analyzed for each sample. Crystals were put in platinium crucibles. He was extracted from apatite and zircon and analyzed using the method developed by *House et al.* [2000]: Pt crucibles were heated to 1000°C using a Nd:YAG laser in order to extract the He which was then analyzed using an isotope dilution (^{3}He spike) quadrupole mass spectrometry system. Apatite aliquots were then dissolved in HNO_3, while zircon aliquots were dissolved in ultrapure lithium metaborate. U and Th concentrations of the apatite and zircon grains were then measured by inductively coupled plasma mass spectrometry measurement (ICP-MS) at the California Institute of Technology. Optical observation of induced fission track distribution on external detectors from fission track samples suggests that U zoning in all apatite grains is minimal. Thus α-ejection corrections (F_T), which assume homogeneous U and Th distributions, should be accurate [*Farley et al.*, 1996; *Jolivet et al.*, 2003].

represents the mean value of 50–100 measurements. Determination of the D_{par} value may be slightly different from one operator to the other [*Ketcham et al.*, 2009]. However, the error should be small enough to be considered negligible [*Sobel and Seward*, 2010].

[22] The annealing model of *Ketcham et al.* [1999] used in this study relies on track lengths and D_{par} measured after etching by a 5.5 M HNO_3 acid during 20 s [*Donelick et al.*, 1999], whereas we used the 1.6 M HNO_3 acid/45 s etching protocol. While the etching parameters can be controlled well enough to have only a negligible effect on the measured mean fission track length, they do have a strong effect on the D_{par} value [*Sobel and Seward*, 2010]. For that reason we corrected the measured D_{par} values following the method of *Sobel and Seward* [2010] to fit with the annealing model of *Ketcham et al.* [1999]. The correction factor is 0.825, and both measured and corrected D_{par} values are reported in Table 2.

[23] The HeFTy software requires temperature-time constraints as input parameters in order to guide the model into defining a temperature-time history for the sample. The constraints are entered as temperature intervals positioned at a chosen time. When running, the model has to pass through that interval. In order to prevent forcing the model into a largely preconstrained cooling pattern, we chose to minimize the input temperature-time constraints. They have been chosen as follows: a first constraint was placed around the fission track age of the sample, running from 140°C to 50°C and thus crossing the entire apatite partial annealing zone (PAZ) [e.g., *Green et al.*, 1989; *Corrigan*, 1991] (see below). If the remaining temperature-time intervals are wide enough to prevent forcing the model, additional constraints can sometimes be placed within the model after an initial run to better refine the cooling history [*Ketcham et al.*, 2000]. These are typically placed around inflection points within the curves calculated during the first run and span the entire PAZ temperature range. The PAZ can be defined as the temperature interval within which the fission tracks anneal at a rate compatible with the geological time scale. It is generally comprised between 110 ± 10°C and 60°C [e.g., *Green et al.*, 1989; *Corrigan*, 1991], but these values can slightly change due to the above mentioned variations in the apatite chemical composition. For temperatures higher than about 110°C, fission tracks will anneal nearly instantaneously compared to the geological time scale, while for temperatures below about 60°C, the annealing rate will be extremely low. For that reason, the annealing models are only valid within the PAZ

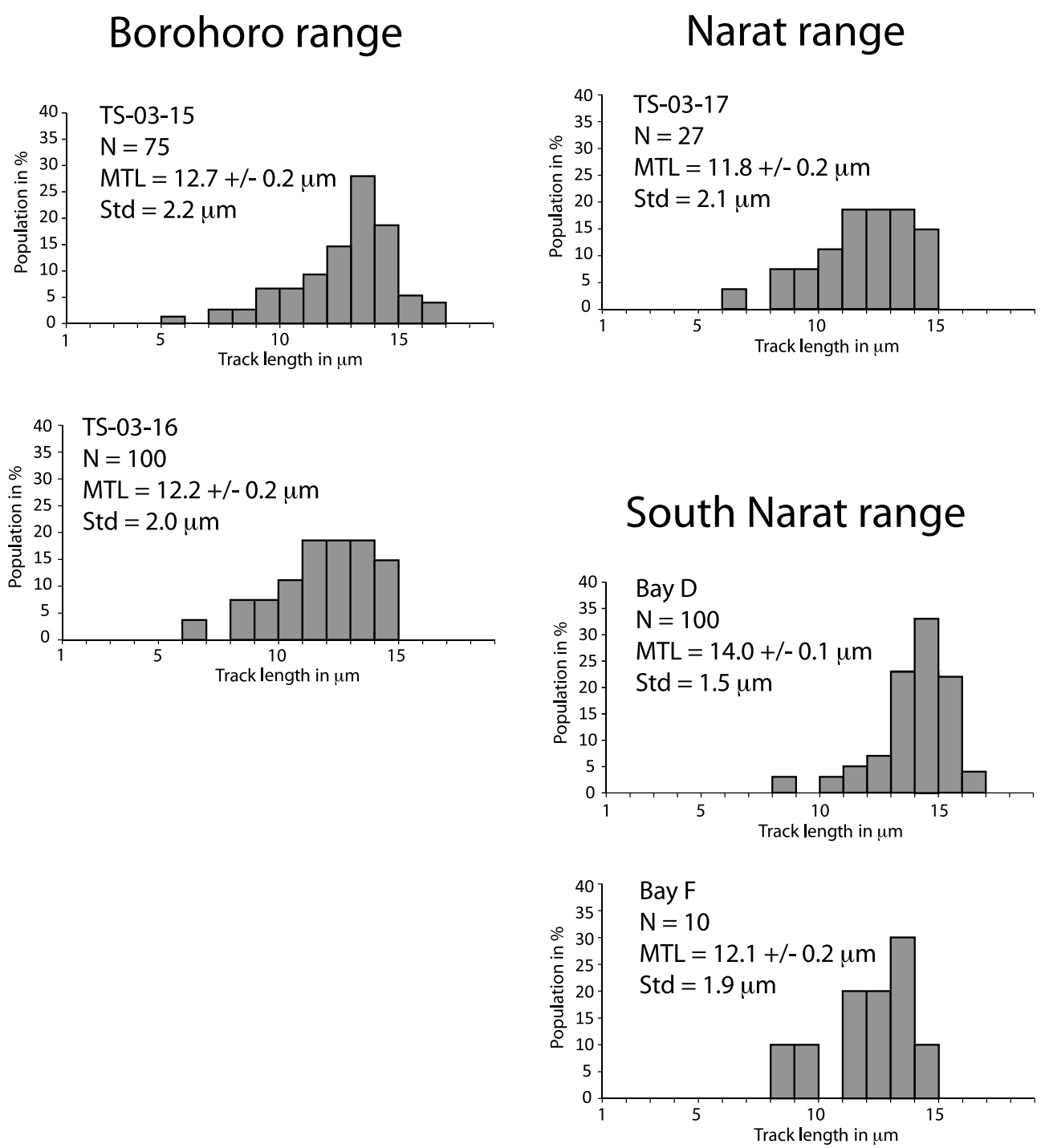


Figure 7. Apatite fission track length distribution histograms for the samples analyzed in this study. The "population in %" is the percentage of lengths in each class. Note that the number of track length measurements (*N*) varies between samples. "MTL" is the mean track length; "Std" is the standard deviation.

temperature range and the portion of the cooling curve obtained outside the PAZ should not be interpreted.

3.1.1. The Borohoro Range and Yili Basin

[24] Samples TS-03-14, TS-03-15, and TS-03-16 show central fission track ages of 34.4 ± 4.4, 69.2 ± 6.5, and 107.3 ± 8.3 Ma, decreasing with increasing altitude. Mean track lengths are 12.7 ± 0.2 μm with a standard deviation of 2.2 μm for TS-03-15 and 12.2 ± 0.2 μm with a standard deviation of 2.0 μm for TS-03-16. Only a very small number of confined horizontal tracks could be measured in sample TS-03-14, and no mean track lengths could be accurately calculated. Corrected D_{par} values vary between 1.6 and 1.9 μm. The track

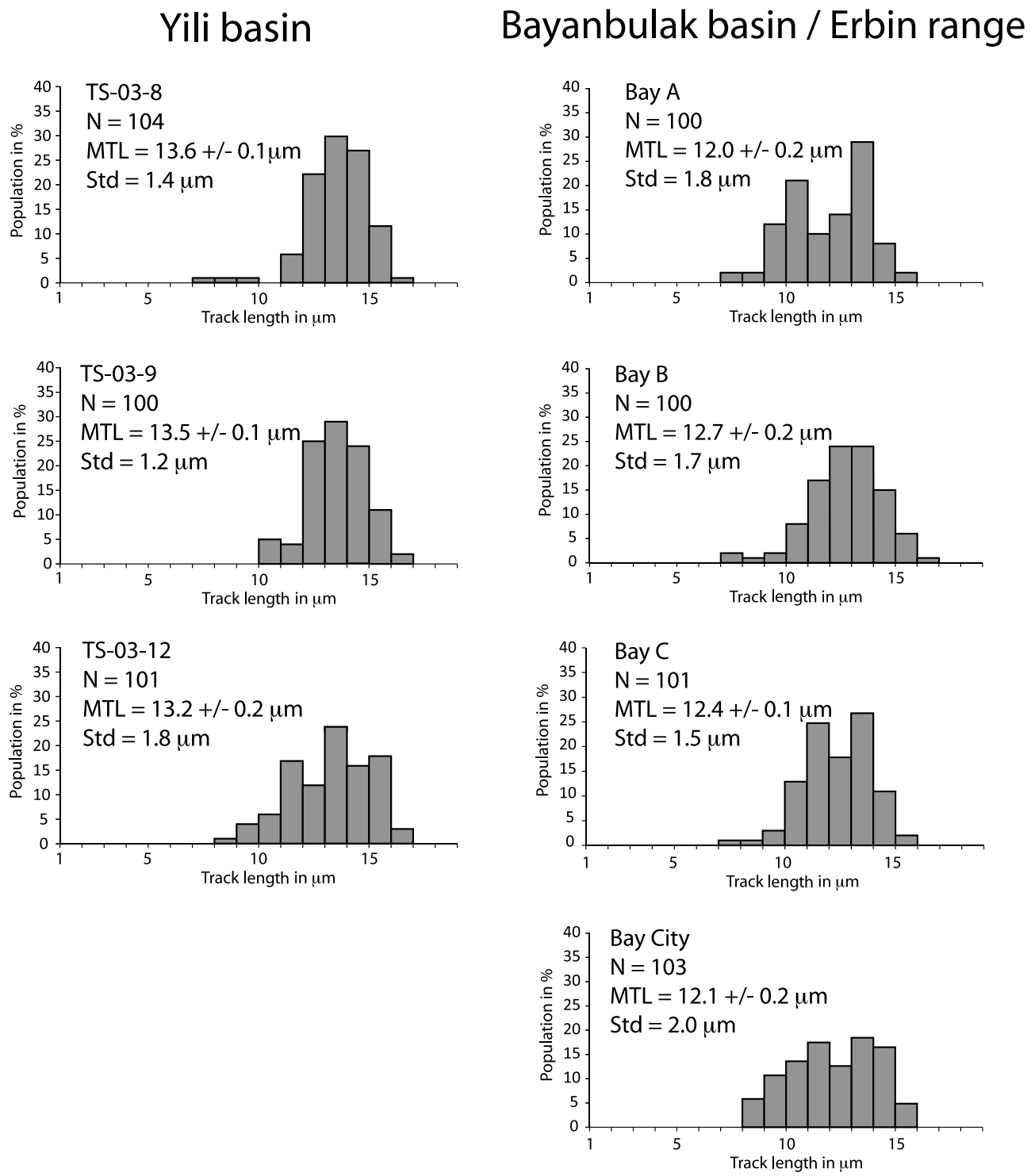


Figure 7. (continued)

length distribution (Figure 7) indicates that while some short tracks are preserved most of the track lengths are comprised between 10 and 15 μm. Associated with the relatively high-standard deviations and the medium mean track lengths, this may be indicative of a slow cooling across the PAZ. Long (>15 μm) tracks in sample TS-03-15 possibly indicate a final, rapid exhumation after a first period of slow cooling [e.g., *Galbraith and Laslett*, 1993].

[25] Samples TS-03-8 to TS-03-12, on both southern and northern sides of the Yili basin, have central fission track ages ranging from 98.3 ± 13.4 to 198.7 ± 35.7 Ma and similar mean track lengths (except for TS-03-10, where mean track lengths could not be calculated owing to the small number of track lengths that could be measured) ranging from 13.2 ± 0.2 to 13.6 ± 0.1 μm. Standard deviations vary from 1.2 to 1.8 μm, smaller than for the samples from the Borohoro range. Corrected D_{par} values are nearly constant between 1.6 and 1.7 μm. The distribution of the track lengths (Figure 7) associated with the high mean track lengths and low standard deviation indicates a rapid cooling through the PAZ. On the southern side of the basin the central ages seem to increase with altitude for samples TS-03-8 to TS-03-10 (Tables 1 and 2). On the northern side of the basin, sample TS-03-12, situated at a slightly higher altitude, is younger than the southern samples, probably reflecting a different exhumation history (Table 2 and Figure 2).

[26] Apatite fission track length modeling was performed on all samples from the Borohoro-Yili region (Figure 9) except TS-03-14 and TS-03-10, where not enough track lengths could be measured.

[27] In the Borohoro range, sample TS-03-16 crosses the 110°C isotherm sometime around 150–130 Ma. The cooling rate of sample TS-03-16 decreases around 140–130 Ma, and the sample then cools slowly until it reaches surface temperature. Sample TS-03-15, situated at a higher altitude and more to the north, has a very different cooling history. The model indicates that sample TS-03-15 remains close to the 110°C isotherm from at least 200 Ma to about 60–65 Ma. This relatively isothermal stage is followed by an obvious increase in cooling rate that brings the sample to the upper part of the PAZ by 60–50 Ma and possibly to the near surface during Paleocene or early Eocene times (as the modeled cooling ends around 60°C where the model becomes inaccurate).

[28] On the northern edge of the Yili basin, sample TS-03-12 crosses the 110°C isotherm between about 125 and 100 Ma and then cools with a constant rate before leaving the PAZ sometime between 60 and 40 Ma. Sample TS-03-8 was affected by a strong cooling event around 100 Ma that brought the sample to temperatures lower than 60°C between 100 and 80 Ma. Such a strong cooling event is also recorded by sample TS-03-9 but between 175 and 150 Ma, thus much earlier in time. A thrust fault is indicated on the geological map [*XBGMR*, 1973] (Figure 2) between sample site TS-03-8 and sample sites TS-03-9 and TS-03-10. Movements along that fault or similar faults in that area could lead to differential movements between small blocks. This could be an explanation for the discrepancy between the two thermal histories. It also suggests that tectonic movements occurred over a very long period of time spanning from the Lower Jurassic to the end of the Lower Cretaceous.

3.1.2. The Narat Range and the Bayanbulak Basin

[29] In the Bayanbulak basin and the Narat range, the fission track ages can be separated into two groups. Samples Bay A, Bay B, and Bay City from the flat surface of the basin (2400–2500 m) have very consistent ages ranging between 147.2 ± 10.5 and 143.3 ± 14.6 Ma. Mean track lengths vary between 12.0 ± 0.2 and 12.7 ± 0.2 μm with standard deviation comprised between 1.7 and 2.0 μm. Corrected D_{par} values vary between 1.7 and 2.1 μm. Sample Bay C from the same area is slightly older with an age of 182.0 ± 15.4 Ma, a mean track length of 12.4 μm (standard deviation of 1.7 μm), and a corrected D_{par} of 1.7 μm (Table 2). The largely unimodal track length distribution (Figure 7), the medium mean track lengths, and the relatively low standard deviation are indicative of a slow exhumation.

[30] Samples Bay D, Bay E, Bay F, and TS-03-17 from the Narat range have much younger ages. Bay D and Bay F have ages of 65.1 ± 4.8 and 91.6 ± 12.1 Ma, respectively. Sample Bay D has a mean track length of 14.0 ± 0.1 μm with a standard deviation of 1.5 μm. Owing to the bad quality of the apatite crystals (numerous inclusions), only 10 tracks could be measured on Bay F and the values reported in Table 2 for this sample as well as the histogram on Figure 7 are only indicative. The tight track length distribution of sample Bay D (Figure 7) associated with the high mean track length value and the low standard deviation indicates a rapid cooling through the PAZ. Bay F has a corrected D_{par} value of 1.3 μm, slightly lower but within the range of values obtained for the granite samples from the basin (see above samples Bay A, Bay B, Bay C, and Bay City), while Bay D has a higher corrected D_{par} value of 3.1 μm. Again because of the numerous (mostly zircons) inclusions and the high density of fractures inside the crystals, only four grains could be analyzed in sample Bay E, giving an age of 72.7 ± 10.1 Ma and a corrected D_{par} value of 3.1 μm consistent with those for Bay D. For the same reasons, no tracks were measured on that sample. The much higher D_{par} value of samples Bay D and Bay E suggest a different chemical composition (for example, a higher Cl content) of the apatite [*Donelick*, 1993; *Burtner et al.*, 1994; *Barbarand et al.*, 2003], possibly due to the different rock type (tonalite instead of granite) (Table 1). Chemical variation within a similar lithology is also frequent, but this does not seem to be the case for samples Bay D and Bay E, which have the same D_{par} value. The higher D_{par} value of samples Bay D and Bay E implies a different annealing behavior for apatite from these samples that should be taken into account by using the D_{par} parameter when performing the thermal modeling of sample Bay D. In sample TS-03-17 only nine apatite crystals were analyzed and 27 fission track lengths could be measured giving an age of 76.3 ± 13.9 Ma, a mean track length of 11.8 ± 0.2 μm with a standard deviation of 2.1 μm, and a corrected D_{par} of 2.1 μm.

[31] In Figure 8a, the high mean track length value obtained for sample Bay D is effectively correlated to the high D_{par} value. However, samples Bay D and Bay E have the highest D_{par} value but the youngest central ages (Figure 8b), indicating that the difference in age between the samples from the Bayanbulak basin and those from the southern Narat range effectively depends on their thermal history and is not entirely due to compositional variations.

[32] The older ages of 196.6 ± 7.8 Ma (DK61) and 204.9 ± 8.4 Ma (DK55) reported by *Dumitru et al.* [2001] from the Erbin Shan (Figures 2 and 8c) were obtained from samples at higher altitude (2660 and 2710 m). There is no tectonic structure separating those samples in the Erbin Shan from samples Bay City, Bay A, Bay B, and Bay C in the basin, and

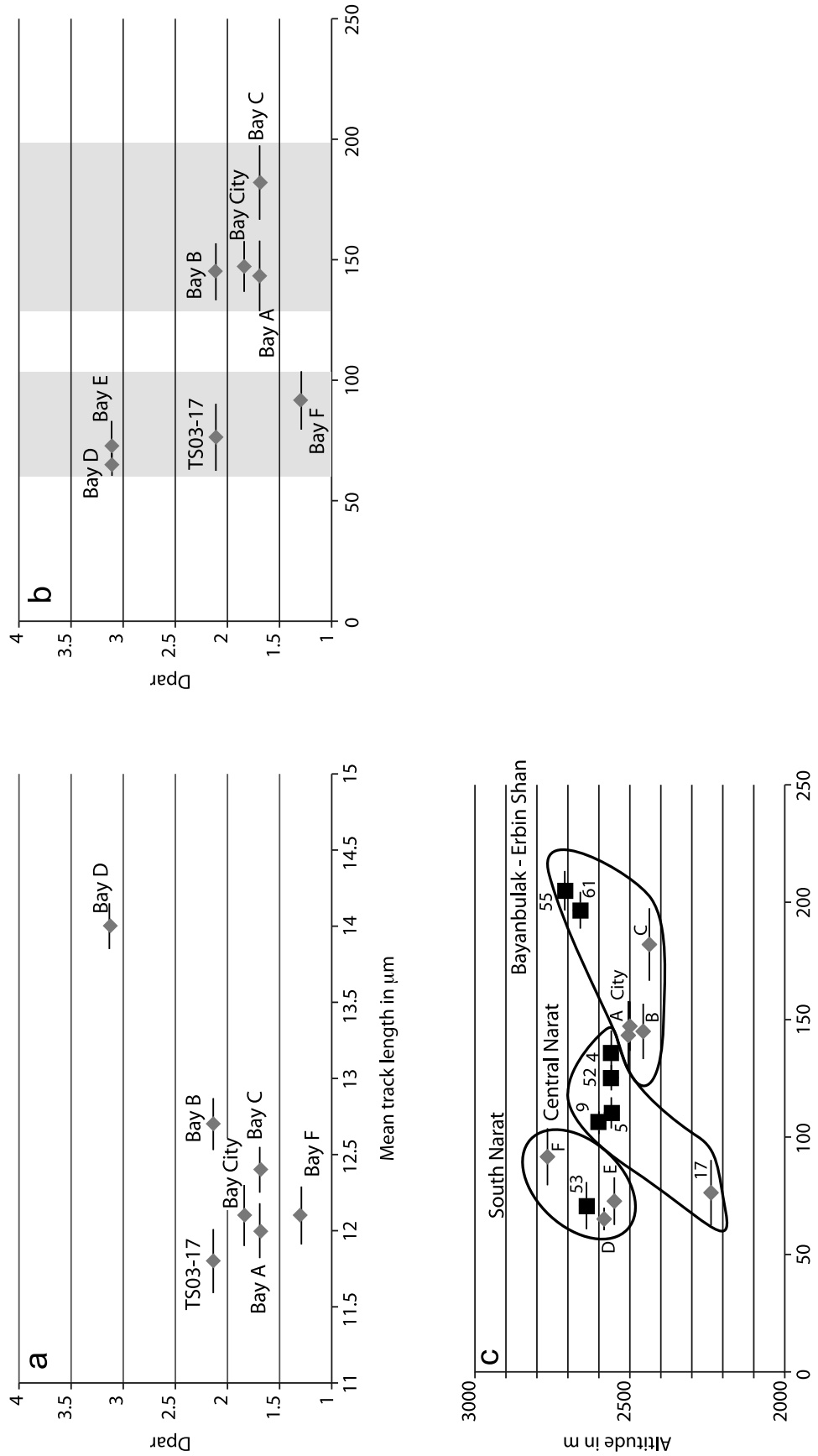


Figure 8. Plots presenting the various apatite fission track data for the Bayanbulak-Narat samples from this study and from *Dumitru et al.* [2001]. (a) Mean track lengths versus D_{par}. (b) Central fission track age versus D_{par}. The two gray shaded areas correspond to the two groups of samples. (c) Fission track ages versus sampling altitude (gray diamonds are samples from this study, black squares are samples from *Dumitru et al.* [2001]). To simplify the labeling, only the final numbers are reported for all samples (for example, 55 stands for DK55). See text for discussion of the data and Table 2 for precise numbers.

Figure 8c shows that they belong to the same group, with the increase in fission track age being correlated with the increase in sampling altitude.

[33] Figure 8c shows the Narat-Bayanbulak data from this study and from *Dumitru et al.* [2001] (Table 2 and Figure 2) plotted on an age-elevation graph. The samples can be separated into three groups (Central Narat, South Narat, and Bayanbulak-Erbin Shan) from their geographic position, and all three groups have a specific age-elevation relation. This is a clear indication that the early Cenozoic exhumation phase was localized within the Narat range and only strongly affected the samples that were close to the actual northern edge of the Bayanbulak basin. Mean long-term exhumation rates derived from the age-elevation graph are very low, on the order of 0.004 mm yr^{-1} for the basin samples and 0.007 mm yr^{-1} for the younger group in the Narat range. These very low rates imply that either the topography of the area remained generally very low during the Mesozoic-Cenozoic period or that the climate conditions did not allow strong erosion. Examples of such low erosion rates have been reported in Mongolia for the same period of time, associated with low topography and a generally dry climate [*Jolivet et al.*, 2007; *Vassallo et al.*, 2007].

[34] Thermal modeling of the apatite fission track data performed on samples where enough track lengths could be measured provides a statistical but more complete temperature time history of the Narat and Bayanbulak area between 110°C and 60°C [e.g., *Green et al.*, 1989; *Corrigan*, 1991]. Models for samples Bay City, Bay B (which are representative models for the basin samples), and Bay D are presented in Figure 10. As already indicated by the distribution of central ages, the oldest samples crossed the 110°C isotherm during a Late Triassic-Middle Jurassic cooling episode. Sample Bay City (Figure 10) and Bay A then remained within the middle to upper part of the PAZ, between 80°C and 60°C until a last cooling event that started around early Eocene times. This last event is only recorded within the upper part of the PAZ, but as its onset temperature is situated around 80°C–70°C and thus inside the confidence interval of the model, we consider this increase in cooling rate as reliable. During the Late Triassic-Middle Jurassic episode, sample Bay B reached the upper part of the PAZ (Figure 10). Samples Bay B and Bay City belong to the same tectonic block, and by comparison with the thermal history obtained for sample Bay City we consider that sample Bay B effectively remained in the upper part of the PAZ during the Upper Jurassic and Cretaceous.

[35] Sample Bay D displays a very different thermal history starting around 60–65 Ma with a rapid cooling through the PAZ from 110°C to 60°C. The model then indicates a long stable period in which the samples remained around 50°C–40°C, but this is only poorly constrained because the thermal modeling can only be considered as valid within the PAZ. Given the rapid initial cooling rate and the concordance between the central fission track age and the time of onset of this cooling, it is reasonable to consider that this sample reached the near surface shortly after 60 Ma. This cooling history is very similar to the one obtained for sample TS-03-15 in the Borohoro range (Figure 9).

3.2. (U-Th)/He Analysis

[36] In order to get a more complete thermal history of the Bayanbulak basin and of the southern edge of the Narat range, we performed (U-Th)/He analysis on zircon and apatite from several characteristic samples. While the apatite fission track data allow constraining the temperature-time history of a sample between about 60°C and 110°C, (U-Th)/He analysi on zircon gives ages corresponding to a closure temperature of 170°C–190°C for common cooling rates and crystal size [e.g., *Reiners et al.*, 2004]. On the other end, the (U-Th)/He method applied to apatite has a closure temperature ranging between 40°C and 85°C depending on the crystal size and the cooling rate [e.g., *Wolf et al.*, 1998; *Farley*, 2000]. ^{4}He nuclei are mostly produced by decay of ^{238}U, ^{235}U, and ^{232}Th within the crystals (some may also derive from ^{147}Sm decay, but this can be considered as negligible, except for Sm-rich minerals) [e.g., *Farley et al.*, 1996; *Farley*, 2000]. Those particles are emitted with enough kinetic energy that they travel for several microns before stopping. This stopping distance of about 20 μm in apatite [e.g., *Ziegler*, 1977; *Farley et al.*, 1996] can induce loss of ^{4}He particles by ejection outside the crystal. This effect can be corrected using the F_T parameter which depends on the shape and size of the analyzed crystal [*Farley et al.*, 1996] (Table 3).

[37] Given their closure temperatures, the (U-Th)/He thermochronometers are thus used to complement the thermal history obtained from the apatite fission track data.

[38] Results are presented in Table 3 as is a complete description of the protocol of analysis in the footnote. All ages discussed below are corrected ages given with their 2σ uncertainty estimated to 6% (due to an analytical uncertainty of 2% for He, U, and Th measurement) [e.g., *Wolf et al.*, 1998; *House et al.*, 1997; *Reiners et al.*, 2000].

3.2.1. Zircon Results

[39] Four samples were analyzed using (U-Th)/He on zircon. Two samples were selected from the northern edge of the Bayanbulak basin in the Narat range (Bay D and Bay F) based on their much younger apatite fission track ages and the peculiar thermal history derived from modeling the apatite fission track data obtained on sample Bay D. The other two samples (Bay A and Bay B) were selected as representative of the basin (see Figure 2 for location). For samples Bay A and Bay D, corrected ages are spread (Table 3 and Figure 11), most probably because of undetectable U or Th sources inside the selected crystals (small size mineral or fluid inclusions, for example). The 567 Ma age obtained for sample Bay D can be excluded, for it is much older than the Late Ordovician

Figure 9. Fission track length modeling for Yili and Borohoro samples. *N*, number of track lengths measured; MTL, mean track lengths in μm; Std, standard deviation on MTL; FT age, central apatite fission track age in Ma. The dark gray shaded envelope corresponds to the good fits, and the light gray envelope corresponds to the acceptable fits. The dashed line corresponds to the best fit. The dashed box indicates the apatite partial annealing zone. Models are only valid within this temperature range. See text for discussion of the results and Table 2 for precise numbers.

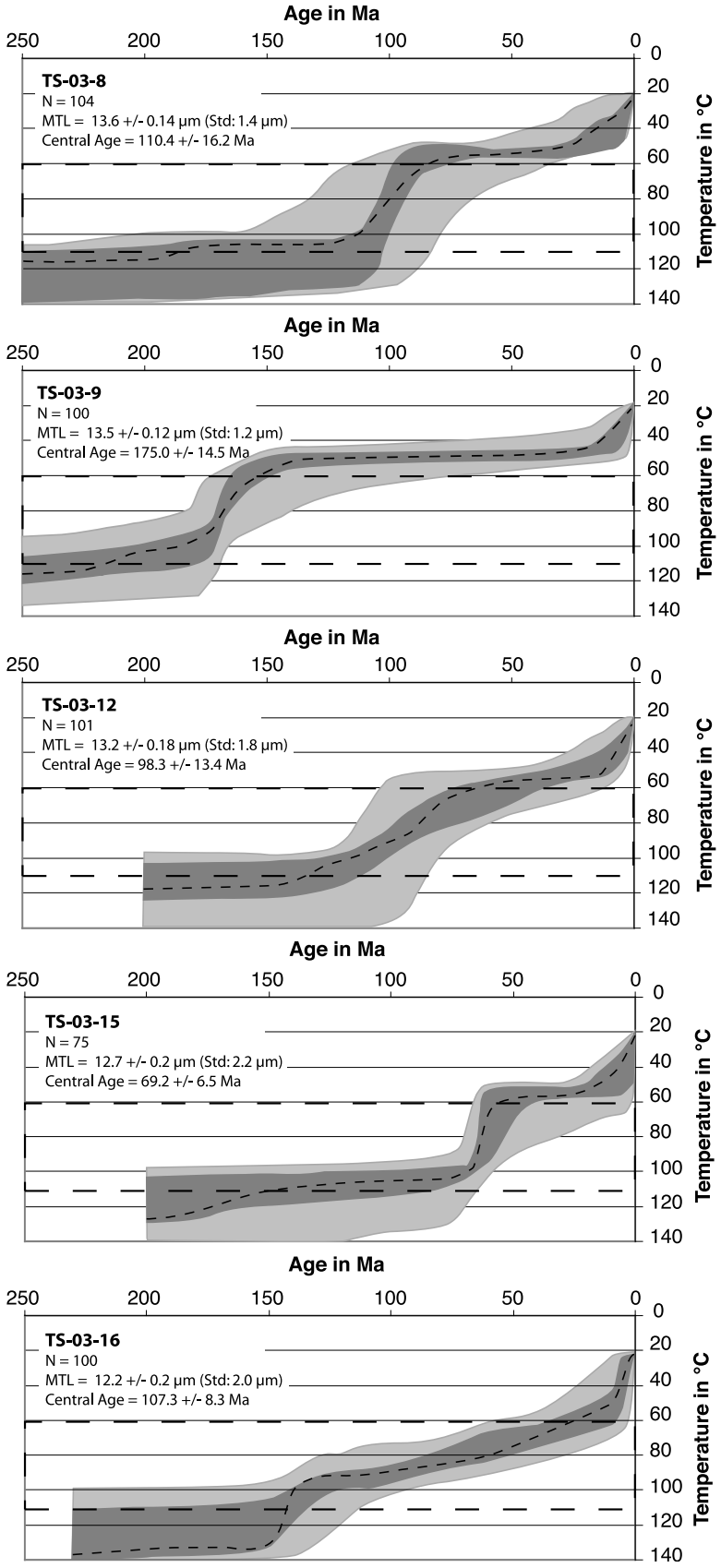

Age in Ma
250
200
150
100
50
0
Temperature in °C
0
20
40
60
80
100
120
140
TS-03-8
N = 104
MTL = 13.6 +/- 0.14 µm (Std: 1.4 µm)
Central Age = 110.4 +/- 16.2 Ma
TS-03-9
N = 100
MTL = 13.5 +/- 0.12 µm (Std: 1.2 µm)
Central Age = 175.0 +/- 14.5 Ma
TS-03-12
N = 101
MTL = 13.2 +/- 0.18 µm (Std: 1.8 µm)
Central Age = 98.3 +/- 13.4 Ma
TS-03-15
N = 75
MTL = 12.7 +/- 0.2 µm (Std: 2.2 µm)
Central Age = 69.2 +/- 6.5 Ma
TS-03-16
N = 100
MTL = 12.2 +/- 0.2 µm (Std: 2.0 µm)
Central Age = 107.3 +/- 8.3 Ma

Figure 9

intrusion age of the tonalite (Table 1) [*Ma et al.*, 1993; *Che et al.*, 1994; *Zhou et al.*, 2001]. Similarly, the 96 Ma age obtained for sample Bay A is much younger than the apatite central fission track age (143 ± 15 Ma) and can thus be excluded although we have no clear explanation for this discrepancy between the ages.

[40] F_T values for the remaining aliquots vary between 0.73 and 0.91, and individual ages are still widely spread between 186 and 328 Ma (Table 3). However, the mean sample ages are comprised between 267 and 286 Ma, implying that the samples reached the 170°C–190°C temperature range around that time [*Reiners et al.*, 2004].

[41] These ages are consistently older than the corresponding apatite fission track ages, and the mean ages are similar to Permian $^{40}Ar/^{39}Ar$ ages on K-feldspars and biotite reported throughout the range [e.g., *Yin et al.*, 1998; *Zhou et al.*, 2001]. K-feldspar from sample DK55 in the Erbin range (Figure 2) gave a $^{40}Ar/^{39}Ar$ spectrum with a maximum age of 278 Ma and a minimum age of 245 Ma [*Zhou et al.*, 2001]. The closure temperature of $^{40}Ar/^{39}Ar$ on K-feldspar spans from 130°C to 250°C [*Lovera et al.*, 1989; *Lovera*, 1992] and thus encloses the closure temperature for (U-Th)/He on zircon. Furthermore, *Hu et al.* [1986] obtained a U/Pb crystallization age of 378 Ma for the Erbin range granite which provides a maximum age limit for this sample and probably for the other granites that we sampled inside the Bayanbulak basin. We will thus consider the zircon ages between 186 and 328 Ma to be reliable. The mechanism that generated the Permian-Early Triassic $^{40}Ar/^{39}Ar$ ages in the Erbin range is still debated between thermal disturbance by late Carboniferous-Early Permian magmatism in the Borohoro [*Zhou et al.*, 2001] and strong erosion [*Dumitru et al.*, 2001].

3.2.2. Apatite Results

[42] Two samples (Bay A and Bay B) from the Bayanbulak basin were analyzed and show ages ranging from 150.3 to 110.9 Ma (four aliquots with a mean value of 133.6 Ma) for Bay A and from 168.9 Ma to 121.2 Ma for Bay B (two aliquots with a mean value of 145.1 Ma), with F_T values of 0.8–0.72 and 0.77–0.74, respectively (Table 3). Owing to the occurrence of numerous zircon and other unknown inclusions in the apatite crystals of samples Bay E and Bay F (see the discussion of apatite fission track data in section 3.1), Bay D was the only sample from the northern edge of the basin to be analyzed. (U-Th)/He ages range from 34.5 to 58.9 Ma (four aliquots with a mean value of 43.9 Ma) with F_T values of 0.70–0.82 (Table 3). In samples Bay A and Bay B, one aliquot gives a (U-Th)/He age older than the apatite central fission track age. This can be due to excess He from small He-rich inclusions within the apatite crystals [e.g., *Farley et al.*, 1996; *Warnock et al.*, 1997] or to ^{4}He trapping within defects in the crystal lattice [*Shuster et al.*, 2006]. Numerous examples of inconsistency between apatite (U-Th)/He and fission track ages (the (U-Th)/He ages are older than the corresponding fission track ages) have recently been exposed in the literature [e.g., *Persano et al.*, 2002; *Belton et al.*, 2004; *Lorencak et al.*, 2004; *Söderlund et al.*, 2005; *Green and Duddy*, 2006]. On the basis of ^{4}He diffusion experiments in apatite crystals, *Shuster et al.* [2006] showed that there is a positive linear correlation between the closure temperature of the He system and log [^{4}He]. This result implies that the diffusion kinetics of ^{4}He in apatite depends not only on temperature but also on the ^{4}He concentration within the mineral and, thus, on any parameter that can increase or decrease this concentration through time. The thermochronology methods based on noble gases such as He and Ar rely on models of the diffusion of radiogenic isotopes inside the crystal lattice [e.g., *McDougall and Harrison*, 1988; *Lovera et al.*, 1989, 1991; *House et al.*, 1999; *Farley et al.*, 1996; *Farley*, 2000]. The calculation of an age using those models depends upon two very strong assumptions: (1) diffusion kinetics of the isotope within the crystal lattice is only controlled by temperature and (2) the diffusion parameters established at high temperature in the laboratory can be extrapolated to the lower temperature and longer time scales involved in geological processes. The results of the diffusion experiments of *Shuster et al.* [2006] imply that when [^{4}He] increases through time (for example, when the temperature becomes very low) the ^{4}He diffusion becomes slower. At low temperature (<60°C), the accumulation of defects within the crystal lattice (such as fission tracks) creates traps in which ^{4}He is retained in a gas-like state. The energy required for the ^{4}He particle to overcome the defect is greater than the normal activation energy required for diffusing within the undisturbed crystal lattice. The diffusion rate will thus decrease with the increasing number of crystal defects until the latter become so numerous that they connect with each other and the external surface of the crystal, creating drains for the ^{4}He [*Shuster et al.*, 2006]. This He-trapping phenomenon induces an overestimation of the apatite (U/Th)He age. *Green and Duddy* [2006] have shown that this situation was occurring mainly when apatite fission track ages become older than about 100 Ma. However, if He trapping was responsible for the old apatite (U-Th)/He ages obtained from samples Bay A and Bay B, one could expect that all the aliquots would have such an old age for all the apatite crystals experiencing the same cooling history and have the same general chemical composition. We thus consider that the old ages are due to excess He from inclusions and that only the aliquots with ages younger than the apatite fission track age should be considered.

[43] Figures 10 and 11 show the consistency between the zircon and apatite (U-Th)/He ages and the apatite fission track ages. Apatite He ages are only slightly younger than apatite central fission track ages, while zircon He ages are much older. This is consistent with a long period of slow cooling during the Mesozoic-early Cenozoic followed by renewed exhumation during the late Cenozoic.

4. Interpretation and Discussion

4.1. Late Paleozoic and Mesozoic Thermal History

[44] Zircon (U-Th)/He analyses from the Bayanbulak basin indicate cooling below 190°C in Early Permian times (about 270–290 Ma). This cooling phase could be reasonably attributed to the effects of the Tarim-Central Tian Shan and North Tian Shan collision [*Allen et al.*, 1993b; *Carroll et al.*, 1995; *Dumitru et al.*, 2001; *Wartes et al.*, 2002]. Indeed, several recent geochronological studies have constrained and dated this major collision event. Numerous Early Permian (295–280 Ma from U/Pb on zircon) postcollisional

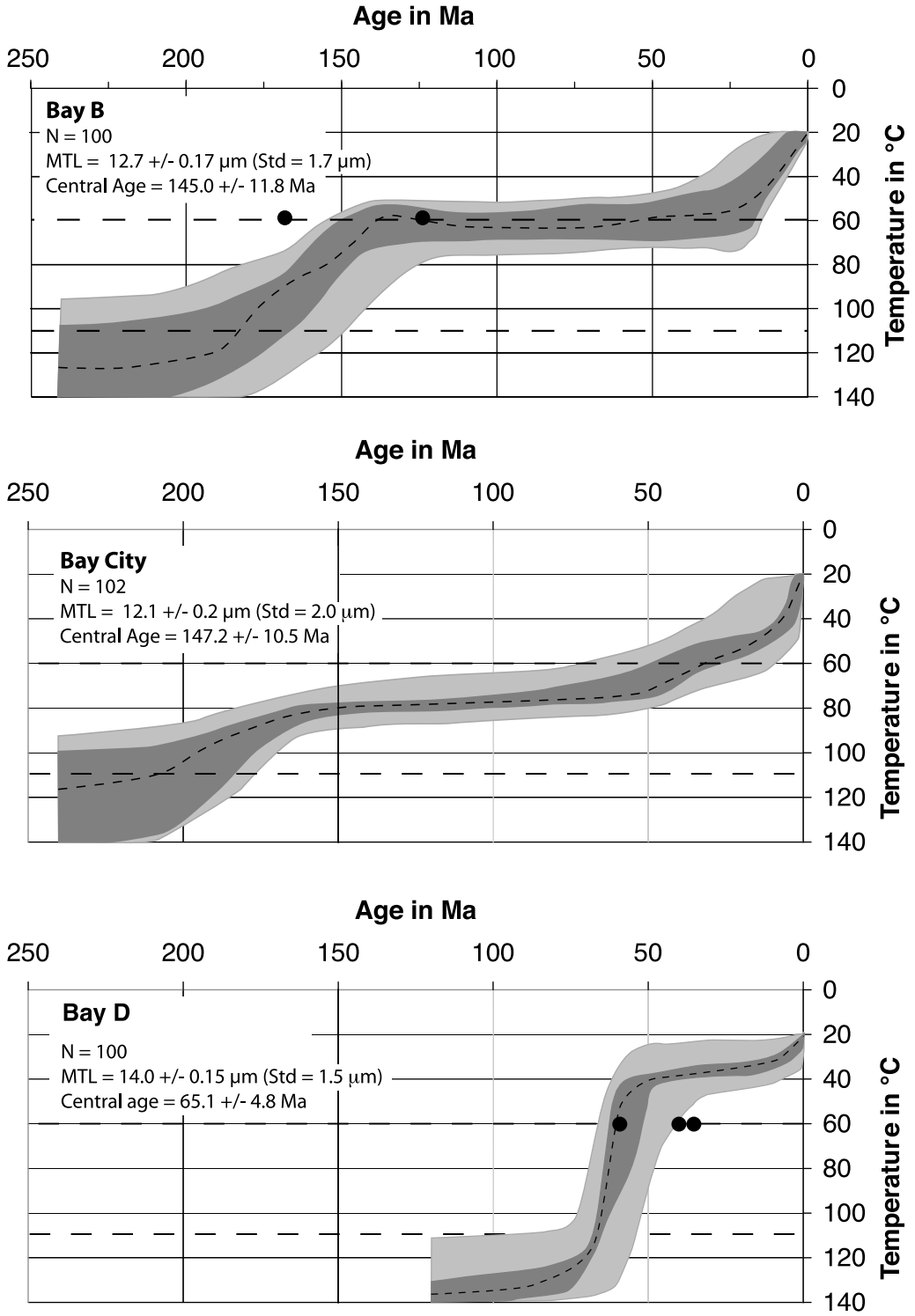


Figure 10. Fission track length modeling for representative samples of the Bayanbulak basin and southern Narat range. Individual apatite (U-Th)/He ages have been reported on the graph (black dots) for samples Bay B and Bay D (they are not available for sample Bay City). *N*, number of track lengths measured; MTL, mean track lengths in μm; central age, central apatite fission track age in Ma. See text for discussion of the results and Tables 2 and 3 for precise numbers.

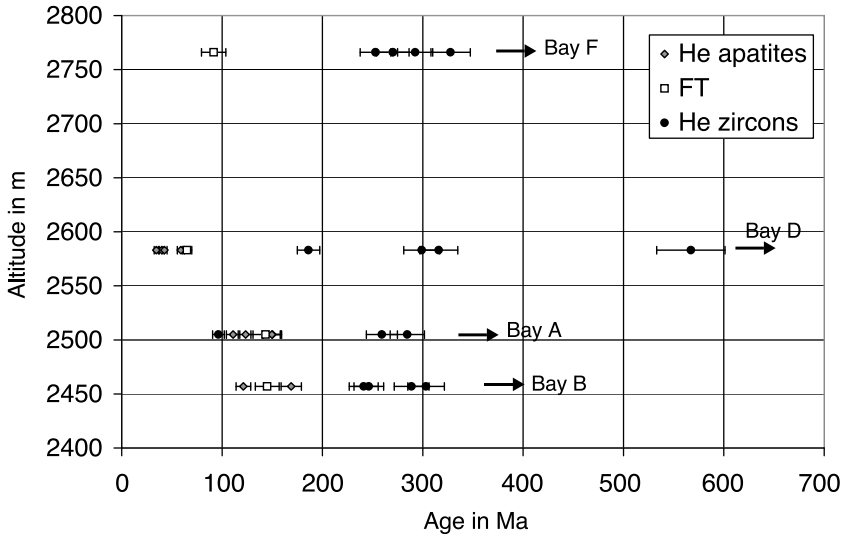


Figure 11. Individual apatite and zircon (U-Th)/He ages as well as central apatite fission track ages plotted against altitude for the Bayanbulak samples. See text for discussion.

A-type granitoids associated with various mafic and Si-undersaturated alkaline rocks are spread all over western Tian Shan, crosscutting the regional Paleozoic structures [e.g., *Konopelko et al.*, 2007; *Gao et al.*, 2009; *Wang et al.*, 2009; *Glorie et al.*, 2010]. This magmatism is interpreted as resulting from mixing of asthenospheric mantle (underplating the Tarim margin) and crustal sources in the Tarim Mesoproterozoic crust [*Konopelko et al.*, 2007]. Ascent of the asthenospheric mantle into the lithosphere would have been favored by major lithospheric structures such as the major east-west strike-slip faults that are still preserved inside the range and were active after the final closure of the Paleo-Turkestan ocean [*Konopelko et al.*, 2007; *Wang et al.*, 2009]. $^{40}Ar/^{39}Ar$ dating of strike-slip fault activity along the Main Tian Shan Shear Zone gives ages of 269 ± 5 Ma (*Shu et al.* [1999] on newly formed muscovite), 250 ± 0.5 Ma (*Chen et al.* [1999] on biotite), and 269 ± 5 and 245 ± 3 Ma (*Laurent-Charvet et al.* [2002] on muscovite and biotite, respectively). $^{40}Ar/^{39}Ar$ dating of granite bodies within the Nikolaev line or Carboniferous sediments immediately south of the fault zone also yielded ages of 263 ± 1 Ma (plateau age on biotite) and 252–253 Ma (plateau ages on white micas and biotite), respectively [*de Jong et al.*, 2009; *Wang et al.*, 2010]. Other geochronological studies (K-Ar and $^{40}Ar/^{39}Ar$) carried out on samples scattered in the range also provided Permian cooling ages [*Yin et al.*, 1998; *Zhou et al.*, 2001].

[45] However, as already shown by *Dumitru et al.* [2001], the cooling episode revealed by medium to low-temperature thermochronology significantly postdates the currently favored Early Permian estimates for the age of the collision. Apatite fission track length modeling indicates that samples from the Bayanbulak basin, the northern edge of the Narat range, and the southern flank of the Borohoro range crossed the 110°C isotherm during Early Jurassic and slowly cooled to temperatures between 80°C and 60°C by Middle Jurassic time. It thus appears that the Permian exhumation phase related to the Tarim-Central Tian Shan and North Tian Shan collision has been overprinted by a subsequent Early Jurassic cooling phase most probably related to continental collisions that occurred farther south in the present-day Tibet plateau region [e.g., *Jolivet et al.*, 2001; *Roger et al.*, 2010]. Samples that are at present-day located in "stable areas" not affected or only slightly affected by the Tertiary deformation still preserved that signal.

[46] Evidence for a widespread Early Jurassic cooling process associated with tectonic movements probably induced during the so-called Cimmerian orogeny by collision between the Qiantang and Kunlun blocks [e.g., *Matte et al.*, 1996; *Roger et al.*, 2008] has been reported in North Tibet [e.g., *Sobel*, 1995; *Sobel and Arnaud*, 1996; *Delville et al.*, 2001; *Jolivet et al.*, 2001]. In the Tian Shan, Tarim, and Junggar those tectonic events led to the reactivation of inherited Paleozoic structures [*Hendrix et al.*, 1992; *Allen and Vincent*, 1997; *Allen et al.*, 2001; *De Grave et al.*, 2007]. Associated with relief building and enhanced erosion, a discordance level is observed in the Tarim basin between Late Triassic and Early Jurassic sediment series [e.g., *Sobel and Arnaud*, 1999; *Vincent and Allen*, 1999]. Late Triassic-Early Jurassic conglomerates as well as an angular unconformity at the base of the Jurassic are also observed at the eastern margins of the Junggar basin [*Vincent and Allen*, 2001]. The continuous cooling observed on the Bayanbulak samples from about Early Permian to Middle Jurassic times might thus be related to a persistent deformation induced by successive block accretion to the south and west of the Tian Shan [e.g., *Roger et al.*, 2008].

[47] However, it is less clear whether the localized cooling we observed in our data during the lower Cretaceous, especially in the Yili basin, can be related to tectonic events to the south. Indeed, the thermochronology record of the Late Jurassic-Early Cretaceous accretion of the Lhasa block [e.g., *Girardeau et al.*, 1984; *Murphy et al.*, 1997; *Gaetani*, 1997] south of the Qiangtang is still debated [e.g., *Roger et al.*, 2010]. The long-term cooling histories obtained on

Mesozoic granites from the whole Songpan-Garzê-Yidun-Longmen Shan region are all similar and show a very slow and regular cooling during the Jurassic and Cretaceous, incompatible with the occurrence of a major tectonic event between circa 150 and 30 Ma [*Xu and Kamp*, 2000; *Kirby et al.*, 2002; *Huang et al.*, 2003; *Roger et al.*, 2004; *Reid et al.*, 2007; *Lai et al.*, 2007; *Zhou et al.*, 2008; *Roger et al.*, 2010]. In North Tibet, the Jurassic cooling that corresponded to the accretion of the Qiangtang block was followed by a protracted period of thermal stability during Late Jurassic and Cretaceous [e.g., *Jolivet et al.*, 2001]. During the same period an extensive peneplanation surface developed in western Central Asia, implying a long period of tectonic quiescence [*Vassallo et al.*, 2007; *Jolivet et al.*, 2007, 2009]. However, Early Cretaceous conglomerates and coarse sediments, mostly contemporaneous with the Lhasa block accretion, are exposed north and south of the Tarim basin as well as in the south Junggar basin, linked with basin-vergent thrusting in the Tian Shan and possibly in the Kunlun Shan [*Hendrix et al.*, 1992; *Sobel*, 1999; *Hendrix*, 2000; *Li et al.*, 2004]. Unlike the geochronological data, this suggests that tectonic activity did occur around the Tarim basin by that time. Nonetheless, the lack of evidence in Tibet for strong deformation related to the Lhasa-Qiangtang collision suggests that another, far-field contemporaneous geodynamic process such as the closure of the Mongol-Okhotsk ocean to the east [e.g., *Enkin et al.*, 1992; *Metelkin et al.*, 2004, 2007] may be responsible for the Early Cretaceous deformation around the Tarim. To the north, in the Siberian Altai, cooling seems to occur from Late Jurassic to late Early Cretaceous while a period of isothermal stability is only registered between the Late Cretaceous and the early Neogene [*De Grave and Van den haute*, 2002; *De Grave et al.*, 2007, 2009]. The authors relate the Late Jurassic-Cretaceous cooling with the closure of the Mongol-Okhotsk ocean and the following collision of the Siberian and Amur continents in the Jurassic-Early Cretaceous [*Enkin et al.*, 1992; *Kravchinsky et al.*, 2002; *Metelkin et al.*, 2004, 2007]. The compressive deformation associated with the closure of the Mongol-Okhotsk ocean affected a large area encompassing the northern Altai range [*De Grave and Van den haute*, 2002], the whole Sayan ranges [*Jolivet et al.*, 2009], and the Patom range north of Lake Baikal [*Jolivet et al.*, 2009]. However, immediately east of the Tian Shan, the Gobi Altai region in Mongolia does not seem to be affected by this tectonic episode. The crustal structures of the Gobi Altai and the Tian Shan are very similar with large NW-SE oriented strike-slip faults inherited from Paleozoic deformation episodes, and it is difficult to understand why the Tian Shan would be affected by the deformation generated by the closure of the Mongol-Okhotsk ocean while the Gobi Altai would remain untouched.

[48] The strong cooling event registered by sample TS-03-8 and TS-03-12 around 100 ± 10 Ma (Figure 9) appears slightly younger than the age of the Lhasa-Qiangtang collision. However, *De Grave et al.* [2004, 2007] and *Glorie et al.* [2010] report similar ages from the Kyrgyz Tian Shan and Lower Cretaceous (~160–100 Ma) extension linked to post-orogenic collapse is described in southeastern Mongolia [e.g., *Webb et al.*, 1999]. *Ritts and Biffi* [2001] and *Vincent and Allen* [2001] recognized that direct correlation between basin geology and specific tectonic events in northwestern China during the Mesozoic is not obvious. They suggest that a continuous contractional setting as well as localized deformation persisted in the region during the Jurassic and most of the Cretaceous consecutively to the accretion of the various Cimmerian blocks. This could also be the case in the Tian Shan. *Vincent and Allen* [2001] showed that episodic deformation occurred in the Junggar basin over several tens of millions of years after the Late Triassic-Early Jurassic boundary. Apatite fission track results from samples TS-03-8 and TS-03-12 from the Yili basin indicate localized vertical movements in Lower Cretaceous time. These Mesozoic cooling ages are coherent with the presence of clastic Jurassic to Cretaceous sediments in the Hexilagen and Bayanbulak basins. Those sediments attest to both subsidence of the basins and erosion of surrounding relief at that time. However, it will be necessary to understand why such deformations, even localized, did not occur or are not recorded by thermochronology methods in the Tibet area or in the Gobi Altai. The driving mechanism at the origin of the Early Cretaceous cooling observed in our data from the Yili basin and from sedimentological observation around the Tarim basin thus remains to be fully understood.

4.2. Late Mesozoic-Early Cenozoic Cooling Episode

[49] It is clear from the present data set that the Narat range underwent a strong uplift/erosion episode in the late Mesozoic-early Cenozoic. Thermal history modeling on sample Bay D together with the apatite (U-Th)/He ages on this sample indicates that rapid cooling occurred between about 65 and 60 Ma and that the sample probably reached a subsurface position (less than 1 km) by that time (Figure 10 and Table 3). The apatite fission track ages of samples TS-03-17, Bay E, Bay D, and Bay F as well as that of sample DK53 of *Dumitru et al.* [2001] are consistent with this result (Figure 2 and Table 2). However, *Dumitru et al.* [2001] obtained central fission track ages between 138 and 106 Ma from samples north of the Laerdun pass (Figure 2 and Table 2). This suggests that Late Cretaceous-early Paleocene uplift was highly localized within the Narat range along the northern edge of the Bayanbulak basin.

[50] *Laurent-Charvet* [2001] showed that, within the Narat range, several post-Silurian mylonitic zones have been reactivated by late Paleozoic possibly Permian low to medium temperature dextral movements. Detailed mapping shows that the number of gouge zones (Figure 12) inside the former mylonitic corridors tends to increase around the Laerdun pass and to its south. The position of some of these gouges seems to coincide with recent surface scarps although it was not possible to clearly relate them. The southern side of the Narat range, which corresponds to the assumed location of the Nikolaev line, is thus clearly a weak zone constituted by several individual shear zones that have been reactivated several times like many other Paleozoic structures within the Tian Shan range [*Hendrix et al.*, 1992; *Allen and Vincent*, 1997; *Allen et al.*, 2001; *De Grave et al.*, 2007; *Buslov et al.*, 2007]. The latest low-temperature deformation marked by the gouge zones observed in this area could be linked to the Cretaceous fast exhumation event recorded by apatite fission

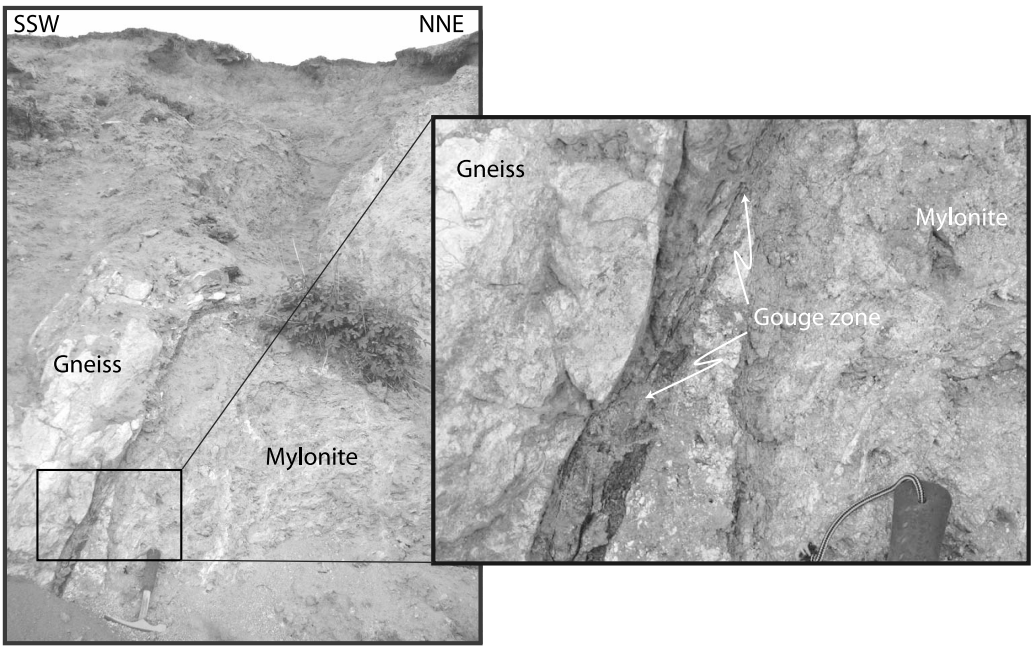


Figure 12. Example of gouge zone along southern flank of the Narat range, south of the Laerdun pass. The roughly E-W trending gouge developed along the contact between a strongly brecciated rock (right) and a competent granitic dyke (left).

tracks and (U-Th)/He thermochronology, and some of these faults have been again reactivated by the ongoing deformation phase.

[51] Evidence for Late Cretaceous-early Paleocene movements in the Borohoro range are fewer but nonetheless obvious. The rapid cooling event recorded by sample TS-03-15 coincides in time with the exhumation phase in the Narat range. As expressed by the Oligocene to late Miocene apatite fission track ages obtained in this study and in the work of *Dumitru et al.* [2001], the highest part of the Borohoro range immediately south of the Hexilagen basin was much more affected by the Cenozoic denudation than was the Narat range. This strong denudation possibly erased most of the late Cretaceous signal. However, as in the Narat range, this denudation event was probably localized on specific structures such as the Main Tian Shan Shear Zone. The inverse fission track age-elevation correlation within the Borohoro range is interpreted as resulting from a southward tilting of the entire range during the Cenozoic. The deformation is accommodated along the south-verging Hexilagen thrust fault (Figure 2) causing the uplift and denudation of the northern part of the South Borohoro range while the southern flank is simply tilted. Following that scenario, the amount of denudation would decrease toward the south until it becomes nearly zero immediately north of the Yili basin. This hypothesis is supported by the difference in erosion style between the northern and southern slopes of the South Borohoro range. While the northern slopes are steep and highly incised, the southern slopes are characterized by a very regular, poorly incised plane-like topography corresponding to a southward tilted flat surface (Figure 13). This surface is incised only when reaching the near summit of the range. Assuming that the Hexilagen fault was activated during the Mesozoic tectonic events, this scenario might have already existed, explaining the early Permian age obtained by *Dumitru et al.* [2001] at the base of the southern slope of the range (Figure 2).

[52] The origin of this Late Cretaceous-early Cenozoic tectonic deformation in the Tian Shan remains uncertain. In Afghanistan, the Kohistan-Dras island arc accreted to Asia in the Middle to Late Cretaceous [e.g., *Searle*, 1991]. In response, a period of accelerated basin subsidence occurred in the north Tarim basin during Late Cretaceous-early Tertiary times, associated with deposition of coarse clastic alluvial sediments. Conglomerates were also deposited during the same time in the south Junggar basin [*Hendrix et al.*, 1992]. In eastern Afghanistan and northwestern Pakistan, major obductions of ophiolites (onto the Kabul block and onto the Indian margin) directly related to the final closure of the Tethys occurred later than the Maastrichtian but before the Middle Eocene, presumably during the Paleogene [e.g., *Tapponnier et al.*, 1981]. The onset of collision with India in the western Himalayas seems to date from the late Ypresian around 50 Ma [*Rowley*, 1996], slightly later than the onset of rapid cooling observed on sample Bay D, and the first large-scale tectonic deformation in the Pamir initiated around late Eocene-Oligocene times, thus later than the cooling event observed on sample Bay D [e.g., *Burtman and Molnar*, 1993; *Arrowsmith and Strecker*, 1999; *Burtman*, 2000; *Coutand et al.*, 2002].

[53] Another driving mechanism for the Late Cretaceous tectonic activity observed in the central part of the Chinese Tian Shan could be linked to the Early Cretaceous closure of the Mongol-Okhotsk ocean and the resulting collision between Siberia and the Mongolia-North China block [e.g., *Enkin et al.*, 1992; *Metelkin et al.*, 2007; *Lin et al.*, 2008]. This

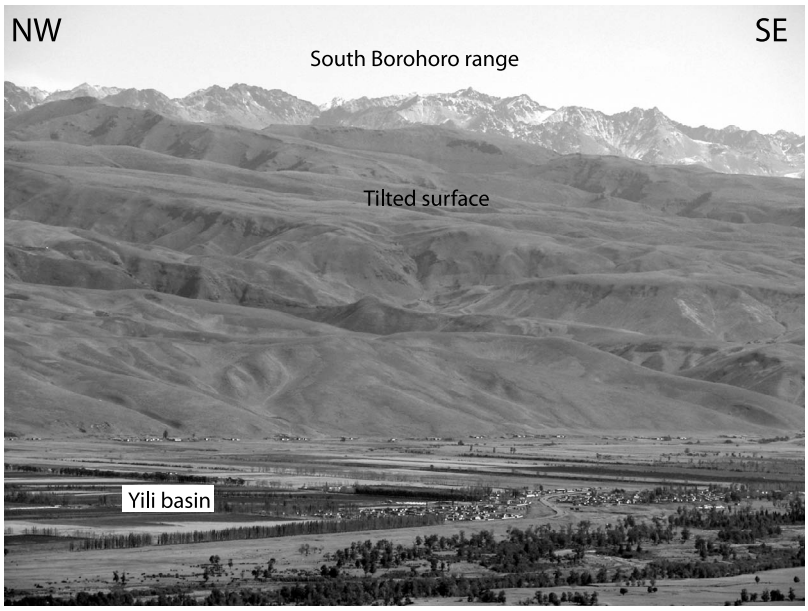


Figure 13. Southern slopes of the South Borohoro range viewed from the Yili basin. The highest part of the range is strongly eroded, mostly by glaciers, but the lowest part of the slope shows a relatively well-preserved tilted flat surface that can be correlated with the surface of the Yili basin. See text for thermochronological and tectonic implications.

continental collision induced a strong thickening of the Mongolian crust, finally leading to postorogenic collapse of the Mongol-Okhotsk belt and the formation of numerous grabens over a huge area extending across the Transbaikal region, southern Mongolia, and northern China [e.g., *Zorin*, 1999; *Webb et al.*, 1999; *Graham et al.*, 2001; *Zorin et al.*, 2002; *Fan et al.*, 2003; *Wang et al.*, 2006]. While the mechanism responsible for the late Late Jurassic-Cretaceous formation of the grabens is still debated [e.g., *Watson et al.*, 1987; *Shao et al.*, 2000; *Ren et al.*, 2002; *Meng*, 2003; *Wang et al.*, 2006], *Jolivet et al.* [2009] have shown that a continuum of deformation probably existed between the orogenic collapse of the Mongol-Okhotsk belt and the early Tertiary initiation of the Baikal Rift Zone in Siberia.

[54] While we cannot demonstrate any direct link between these geodynamic processes (arc collisions to the southwest and orogenic collapse in the east and northeast) and the Late Cretaceous movements in the Tian Shan, the lithosphere of Central Asia was definitely submitted to large-scale deformation at that time. It appears, however, that during the late Cenozoic-early Tertiary the geodynamic mechanisms driving the deformation of the Asian lithosphere originated thousands of kilometers away from the Tian Shan but, as for the present-day India-Asia collision, they had important far-field effects that affected the highly prestructured Tian Shan area.

4.3. Neogene to Quaternary Cooling and Deformation

[55] *Khain* [1985] stated that Cenozoic deformation in the western part of the belt (Kyrgyzstan and Kazakhstan) began in Oligocene time but was predominant during and after Pliocene time. *Allen et al.* [1994] suggested that the basal Oligocene unconformity observed in the Turpan and eastern Tarim basins may mark the initiation of Cenozoic deformation in that region. *Sobel and Dumitru* [1997] concluded from detrital apatite fission track data from the Tarim basin that thrusting in the Tian Shan started around Oligo-Miocene times. These conclusions have been recently complemented by apatite fission track data and sediment studies from the Kyrgyz Tian Shan [e.g., *Bullen et al.*, 2001, 2003; *Sobel et al.*, 2006; *Buslov et al.*, 2007; *Glorie et al.*, 2010] indicating that a phase of rapid cooling initiated in the central part of the range around 11 Ma. A similar acceleration of the exhumation/erosion rate at 11 Ma is shown by magnetostratigraphy data in the northern and southern piedmonts of the Chinese Tian Shan [*Charreau et al.*, 2005, 2006]. This phase followed a possible reheating event during the late Oligocene-Miocene (circa 25–5 Ma) due to an increase in sediment loading indicating renewed erosion of a growing topography [*Glorie et al.*, 2010]. From apatite fission track analysis on the Manas river (northern Tian Shan), *Hendrix et al.* [1994] described a strong tectonic reactivation around late Oligocene-early Miocene times.

[56] In the Narat range, the Yili basin, and the Bayanbulak basin, low-temperature thermochronology does not show clear evidence for such Neogene exhumation, certainly because it remains limited. The fission track and (U-Th)/He data do not provide any constraints on the amount of Tertiary exhumation in the Narat range except that it must be modest enough (less than about 2 km) not to be registered by the low-temperature thermochronometers. Nonetheless some of the summits in that range are characterized by preserved flat erosion surfaces that may correspond, as in Kazakstan or Mongolia [*Allen et al.*, 2001; *Jolivet et al.*, 2007], to preserved remnants of the initial topography. If this is confirmed and if these flat summits are correlated with the Bayanbulak

basin floor, then the total Tertiary surface uplift in the Narat range corresponds to the 1500 m difference in altitude between the summits and the basin floor. This does not create a sufficient exhumation to be registered by apatite fission tracks or even by apatite (U-Th)/He.

[57] However, the Neogene event is well-defined in the Borohoro range, and especially by the high elevation samples immediately south of the Hexilagen basin (Figure 2). As already mentioned above, this can be explained by accommodation of the deformation along the Hexilagen thrust fault which induced a southward tilting of the whole southern Borohoro range leading to strong erosion in the north and nearly no erosion in the south. The Hexilagen fault is part of the north Tian Shan fault system that shows evidence of strong reactivation during Cenozoic times [*Ma*, 1986; *Zhou et al.*, 2001], and *Dumitru et al.* [2001] indicate that this area underwent strong cooling within the past 20 Ma.

[58] It is clear from field observations that active deformation is not only localized on both piedmonts of the Tian Shan range but also occurs in its most central part. In the Yili-Bayanbulak region, the Cenozoic deformation reactivated preexisting basement structures inherited from the Paleozoic history of the range (such as the Nikolaev line). On the northern border of the Bayanbulak basin, this tectonic activity favored the exhumation of the Paleozoic basement, resulting in the uplift of the Narat and Erbin Shan ranges.

[59] During the Quaternary, the deformation affecting the northern part of the Bayanbulak basin propagated toward its center as attested by the occurrence of active folds and thrust faults close to the basin depocenter. This feature strongly suggests that the basin is progressively closing and could completely disappear within the next few million years. A similar scenario is observed in the small Narat basin, in the Yili basin, and in the Hexilagen basin. On a general scale active closure of intramontane basins appears characteristic of the ongoing orogenic process of the Tian Shan range. As shown by many authors [e.g., *Windley et al.*, 1990; *Allen et al.*, 1993b; *De Grave et al.*, 2004; *Buslov et al.*, 2007], the edges of the Turfan basin, Korla basin, Issyk-Kul basin, and many others are all affected by active thrusting, indicating that a significant part of shortening is presently accommodated there. The M_s = 7.3 Suusamyr, Kyrgyzstan, earthquake [*Mellors et al.*, 1997; *Ghose et al.*, 1997] is probably a good example of the seismic activity associated with the closing of such a basin and is well representative of the type of earthquake that could be expected in the Bayanbulak area.

5. Conclusion: General Model of the Deformation Between the Borohoro Range and the Erbin Shan

[60] The thermal evolution associated with the early Mesozoic tectonic history of the Chinese Tian Shan mountain belt is still preserved within the intramontane sedimentary basins and in the internal ranges, allowing a long-term reconstruction of the deformation in that region (Figure 14).

[61] Apatite fission track analysis and (U-Th)/He dating on apatite and zircons show that after an Early Permian to Middle Jurassic episode of general uplift and denudation the Bayanbulak-Yili area underwent a protracted period of very slow cooling from Middle Jurassic to Late Cretaceous (corresponding to a erosion rate between 0.004 and 0.007 mm yr^{-1}) (Figures 14a and 14b). This might be compared with evidence of a similar tectonically quiet period observed in northern Tibet, southern Mongolia, and Siberia during the Jurassic-Cretaceous [e.g., *Jolivet et al.*, 2001, 2007, 2009; *Yuan et al.*, 2006; *Vassallo et al.*, 2007]. Nonetheless, it should be noted that, during the Late Jurassic-Early Cretaceous, cooling still occurred in the northern Altai possibly linked to far-field effects of the closure of the Mongol-Okhotsk ocean. Isothermal stability is then observed in that region from Late Cretaceous to early Neogene [*De Grave and Van den haute*, 2002; *De Grave et al.*, 2007, 2009]. Paleoenvironmental studies in southern Mongolia, northern Tibet, and Tian Shan indicate that these regions were characterized by a warm semiarid to arid climate during the Late Jurassic-Early Cretaceous times [*Hendrix et al.*, 1992; *Wang et al.*, 1999; *Tang et al.*, 2001; *Li et al.*, 2004]. Furthermore, the climate became even drier during the Tertiary [*Ramstein et al.*, 1997; *Wang et al.*, 1999; *Dupont-Nivet et al.*, 2007]. The lack of climate-driven erosion associated with a gener-

Figure 14. Schematic paleogeographic reconstruction for the Bayanbulak basin-Borohoro range region. Vertical and horizontal scales are informative. Only the main structures and the major rock units (without internal details) are reported on the geological section. (a) Permian-Lower Jurassic situation. The collision further to the south of the Qiangtang and Kunlun-Tarim blocks during the Cimmerian orogeny activated the deformation in the Paleo Tian Shan range. Given the widespread occurrence of Jurassic sediments and the multitude of Mesozoic low-temperature thermochronology ages, this tectonic activity must have been quite similar in scale with the current deformation. (b) Late Jurassic-Early Cretaceous. Following the early Mesozoic orogenic episode, the middle Mesozoic period is characterized by erosion and peneplantion of the existing relief. The basins are filled with coal-bearing sediments during the Jurassic before a complete ending of the sedimentation during the Cretaceous probably linked to the absence of erodible relief. (c) Late Cretaceous-Paleogene. Local reactivation of favorably oriented inherited structures is driven by far-field effects of large geodynamic processes affecting the Central Asian lithosphere. Relief building in the Narat range is attested by deposition of coarse conglomerates in the northern Bayanbulak basin, followed by finer clastic sediments. On the basis of our thermochronological results, we assume that the situation might have been similar along the southern margin of the Hexilagen basin. (d) Neogene-Quaternary. By late Oligocene or Miocene, the present-day deformation episode started, reactivating several inherited structures in the range and leading to a block-type deformation. The compressive deformation progressively migrates toward the until-then undeformed center of the endoreic basins, progressively closing them. Finally, the deformation also propagates toward the outside of the Tian Shan range, uplifting for example the North Borohoro range.

ally flat topography, where small-scale smooth relief may be preserved, can explain the nearly complete lack of Cretaceous sediments in the Bayanbulak and adjacent basins. Slow cooling and exhumation of the samples was controlled by wind-driven erosion and slow surface alteration as observed in the present-day Gobi and Taklamakan deserts.

[62] However, in Late Cretaceous, evidence of strong and localized uplift is recorded in the Narat range, and to a smaller scale in the Borohoro range (Figure 14c). However, while Cretaceous sediments have been recognized in the Bayanbulak basin, we have no evidence of such sediments in the Hexilagen basin, possibly because they were erased by erosion. These cooling episodes are probably linked to the reactivation of old inherited structures such as the Nikolaev line or the Hexilagen fault possibly by far-field effects of either the accretion of blocks such as the Kohistan-Dras arc to the southwest or of the extensional processes that affected the lithosphere in the Siberia-Mongolia-North China zone. The origin of the Late Cretaceous movements inside the Tian Shan definitely remains to be understood, but in any case these movements indicate that deformation in the Central Tian Shan is very complex and is localized on preexisting

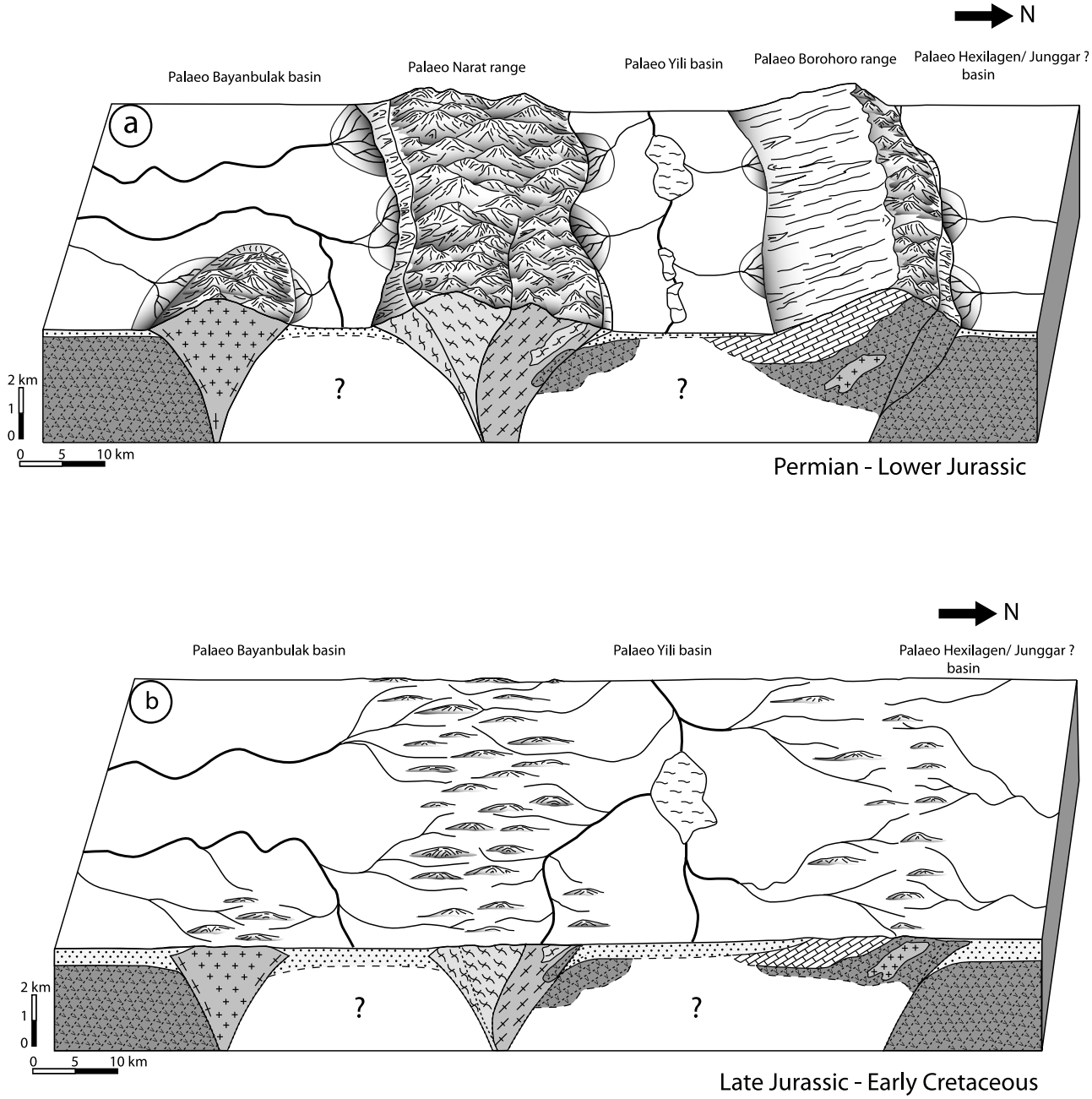


Figure 14

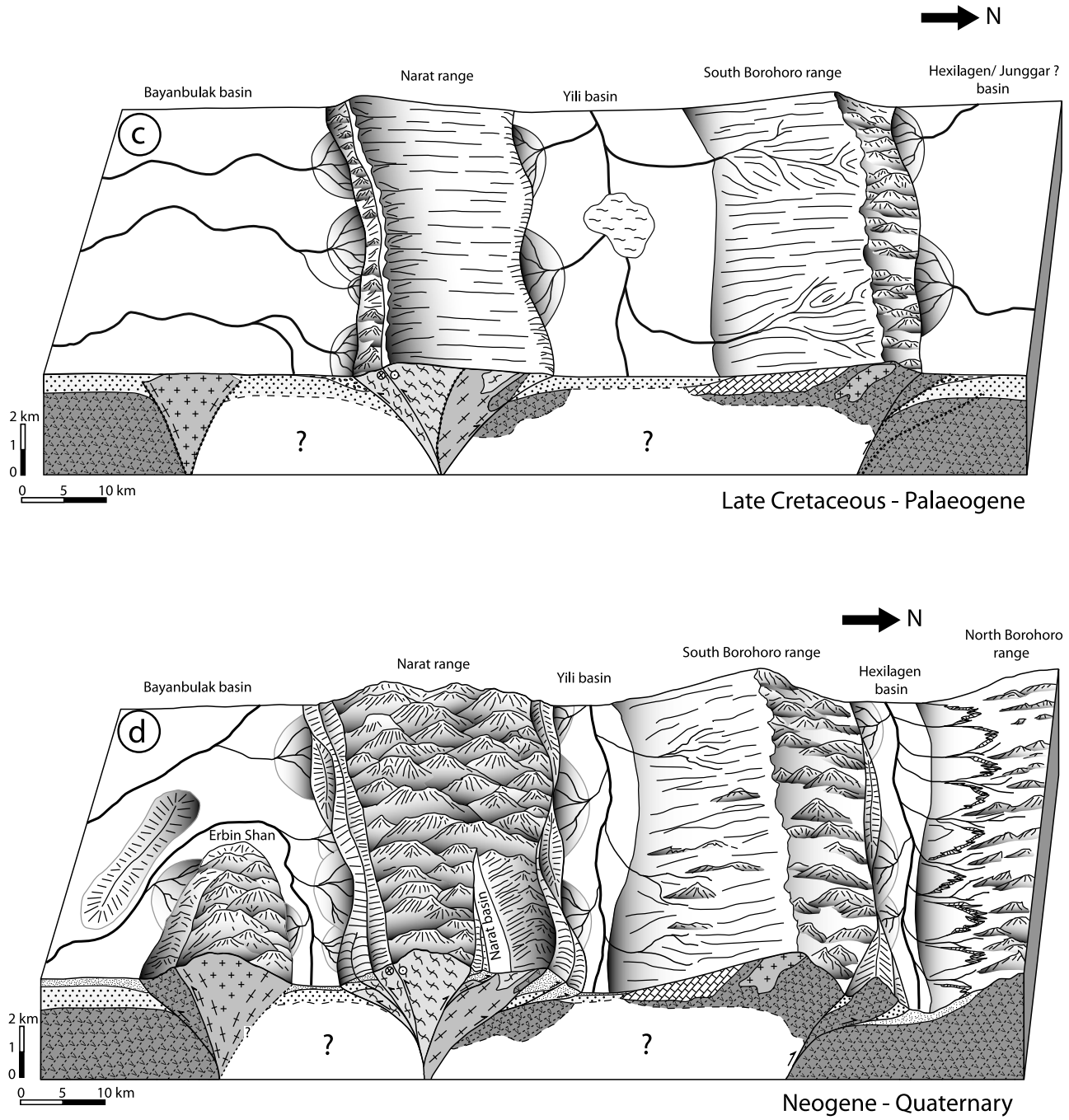


Figure 14. (continued)

structures. Furthermore, our results show that all the observed topography may not be simply the result of the India-Asia collision but could be inherited from earlier tectonic events.

[63] Following the first phase of localized Late Cretaceous uplift, the Tertiary compression linked to the India-Asia collision to the south seems to affect the Yili-Bayanbulak area possibly from around late Oligocene-early Miocene times. This is consistent with the 20–25 Ma age estimated for the onset of deformation in the southern piedmont [e.g., *Sobel and Dumitru*, 1997; *Yin et al.*, 1998]. While the deformation tends to propagate outward toward the Tarim and Junggar basins, part of it is localized along inherited structures. Individual blocks such as the Narat range or the Borohoro range are uplifted and/or tilted to accommodate the compression. Nonetheless, active faulting and folding propagates toward the center of the various intramontane basins that may close completely (Figure 14d). The complete closure of these basins, if realized, may be a major event in the history of the

Tian Shan belt. *Meyer et al.* [1998] proposed that the complete filling of subsequent basins in northern Tibet and the coalescence of their base level with the summit of the surrounding ranges may explain the high altitude but flat topography of the Tibetan Plateau. In Tian Shan, the closure of the intramontane basins will probably impede the internal deformation of the range and accelerate the outward growth of the range.

[64] This study emphasizes the necessity of understanding the Paleozoic and Mesozoic history of the major Asian belts to decipher the Tertiary deformation event. It demonstrates the importance of inherited structures in localizing the first increments of the deformation before it propagates into yet undeformed areas. Finally, it shows that while the actual topography of the Tian Shan range is mainly related to the Tertiary tectonic phase, some of it may be inherited from older, Late Cretaceous-early Tertiary localized tectonic deformation events.

[65] **Acknowledgments.** This work was supported by the French Institut National des Sciences de l'Univers program ECLIPSE (Environnement et Climat du Passé: Histoire et Evolution), and the Agence Nationale pour la Recherche program ANR Blanc 05-0143-01, Chinese project kzcx3-sw-147 and NSFC 40711130402. We thank J.-P. Avouac and K. Farley for their help respectively during fieldwork and (U-Th)/He dating. Mark Allen and an anonymous reviewer provided a constructive review of the initial manuscript.

References

Alexeiev, D. V., H. E. Cook, V. M. Bustyshkin, and L. Y. Golub (2009), Structural evolution of the Ural-Tian Shan junction: A view from Karatau ridge, South Kazakhstan, *C. R. Geosci.*, *341*, 287–297, doi:10.1016/j.crte.2008.12.004.

Allen, M. B., and S. J. Vincent (1997), Fault reactivation in the Junggar region, northwest China: The role of basement structures during Mesozoic-Cenozoic compression, *J. Geol. Soc.*, *154*, 151–155, doi:10.1144/gsjgs.154.1.0151.

Allen, M. B., B. F. Windley, C. Zhang, Z. Y. Zhao, and G. R. Wang (1991), Basin evolution within and adjacent to the Tienshan range, NW China, *J. Geol. Soc.*, *148*, 369–378, doi:10.1144/gsjgs.148.2.0369.

Allen, M. B., B. F. Windley, and C. Zhang (1993a), Palaeozoic collisional tectonics and magmatism of the Chinese Tien Shan, central Asia, *Tectonophysics*, *220*, 89–115, doi:10.1016/0040-1951(93)90225-9.

Allen, M. B., B. F. Windley, C. Zhang, and J. H. Guo (1993b), Evolution of the Turfan basin, Chinese central Asia, *Tectonics*, *12*(4), 889–896, doi:10.1029/93TC00598.

Allen, M. B., B. F. Windley, and C. Zhang (1994), Cenozoic tectonics in the Urumqi-Korla region of the Chinese Tien Shan, *Geol. Rundsch.*, *83*, 406–416.

Allen, M. B., G. I. Aslop, and V. G. Zhemchuzhnikov (2001), Dome and basin refolding and transpressive inversion along the Karatau fault system, southern Kazakstan, *J. Geol. Soc.*, *158*, 83–95, doi:10.1144/jgs.158.1.83.

Arrowsmith, J. R., and M. R. Strecker (1999), Seismotectonic range-front segmentation and mountain-belt growth in the Pamir-Altai region, Kyrgyzstan (India-Eurasia collision zone), *Geol. Soc. Am. Bull.*, *111*, 1665–1683, doi:10.1130/0016-7606(1999)111<1665:SRFSAM>2.3.CO;2.

Avouac, J. P., P. Tapponnier, M. Bai, H. You, and G. Wang (1993), Active thrusting and folding along the northern Tien Shan and late Cenozoic rotation of the Tarim relative to Dzungaria and Kazakhstan, *J. Geophys. Res.*, *98*(B4), 6755–6804, doi:10.1029/92JB01963.

Barbarand, J., A. Carter, I. Wood, and T. Hurford (2003), Compositional and structural control of fission-track annealing in apatite, *Chem. Geol.*, *198*, 107–137, doi:10.1016/S0009-2541(02)00424-2.

Belton, D. X., R. W. Brown, B. P. Kohn, D. Fink, and K. A. Farley (2004), Quantitative resolution of the debate over antiquity of the central Australian landscape: Implications for the tectonic and geomorphic stability of cratonic interiors, *Earth Planet. Sci. Lett.*, *219*, 21–34, doi:10.1016/S0012-821X(03)00705-2.

Biske, Y. S., and R. Seltmann (2010), Paleozoic Tian-Shan as a transitional region between the Rheic and Urals-Turkestan oceans, *Gondwana Res.*, *17*, 602–613, doi:10.1016/j.gr.2009.11.014.

Bullen, M. E., D. W. Burbank, J. I. Garver, and K. Y. Abdrakhmatov (2001), Late Cenozoic tectonic evolution of the northwestern Tien Shan: New age estimate for the initiation of mountain building, *Geol. Soc. Am. Bull.*, *113*, 1544–1559, doi:10.1130/0016-7606(2001)113<1544:LCTEOT>2.0.CO;2.

Bullen, M. E., D. W. Burbank, and J. I. Garver (2003), Building the Northern Tien Shan: Integrated thermal, structural, and topographic constraints, *J. Geol.*, *111*, 149–165, doi:10.1086/345840.

Burbank, D. W., J. K. McLean, M. Bullen, K. Y. Abdrakhmatov, and M. M. Miller (1999), Partitioning of intermontane basins by thrust-related folding, Tien Shan, Kyrgyzstan, *Basin Res.*, *11*, 75–92, doi:10.1046/j.1365-2117.1999.00086.x.

Burtman, V. S. (1975), Structural geology of Variscan Tien Shan, USSR, *Am. J. Sci.*, *275*, 157–186.

Burtman, V. S. (2000), Cenozoic crustal shortening between the Pamir and Tien Shan and a reconstruction of the Pamir-Tien Shan transition zone for the Cretaceous and Paleogene, *Tectonophysics*, *319*, 69–92, doi:10.1016/S0040-1951(00)00022-6.

Burtman, V. S., and P. Molnar (1993), Geological and geophysical evidence for deep subduction of continental crust beneath the Pamir, *Spec. Pap. Geol. Soc. Am.*, *281*, 76 pp.

Burtner, R. L., A. Nigrini, and R. A. Donelick (1994), Thermochronology of lower Cretaceous source rocks in the Idaho-Wyoming Thrust Belt, *AAPG Bull.*, *78*, 1613–1636.

Buslov, M. M., Y. Fujiwara, K. Iwata, and N. N. Semakov (2004a), Late Paleozoic-early Mesozoic geodynamics of Central Asia, *Gondwana Res.*, *7*, 791–808, doi:10.1016/S1342-937X(05)71064-9.

Buslov, M. M., J. De Grave, and E. V. Bataleva (2004b), Cenozoic tectonics and geodynamic evolution of the Tien Shan mountain belt, Himalayan *J. Sci.*, *2*, 106–107.

Buslov, M. M., J. De Grave, E. V. Bataleva, and V. Y. Batalev (2007), Cenozoic tectonic and geodynamic evolution of the Kyrgyz Tien Shan Mountains: A review of geological, thermochronological and geophysical data, *J. Asian Earth Sci.*, *29*, 205–214, doi:10.1016/j.jseaes.2006.07.001.

Carroll, A. R., S. A. Graham, M. S. Hendrix, X. Ying, and D. Zhou (1995), Late Paleozoic tectonic amalgamation of northwestern China: Sedimentary record of the northern Tarim, northwestern Turpan, and southern Junggar basins, *Geol. Soc. Am. Bull.*, *107*, 571–594, doi:10.1130/0016-7606(1995)107<0571:LPTAON>2.3.CO;2.

Carroll, A. R., S. A. Graham, E. Z. Chang, and C. McKnight (2001), Sinian through Permian tectonostratigraphic evolution of the northwestern Tarim basin, China, in *Paleozoic and Mesozoic Tectonic Evolution of Central Asia: From Continental Assembly to Intracontinental Deformation*, edited by M. S. Hendrix and G. A. Davis, *Mem. Geol. Soc. Am.*, 194, 47–69, doi:10.1130/0-8137-1194-0.47.

Charreau, J., Y. Chen, S. Gilder, S. Dominguez, J.-P. Avouac, S. Sen, D. J. Sun, Y. A. Li, and M. W. Wang (2005), Magnetostratigraphy and rock magnetism of the Neogene Kuitun He section (northwest China): Implications for late Cenozoic uplift of the Tianshan mountains, *Earth Planet. Sci. Lett.*, *230*, 177–192, doi:10.1016/j.epsl.2004.11.002.

Charreau, J., S. Gilder, Y. Chen, S. Dominguez, J.-P. Avouac, S. Sen, M. Jolivet, Y. Li, and W. M. Wang (2006), Late Cenozoic erosion history of the Tianshan Mountains as recorded in the Yaha section, Tarim Basin, China, *Geology*, *34*, 181–184, doi:10.1130/G22106.1.

Charvet, J., L. Shu, S. Laurent-Charvet, B. Wang, M. Faure, D. Cluzel, Y. Chen, and K. de Jong (2009), Paleozoic tectonic evolution of the Tianshan belt, NW China, *Sci. China, Ser. D Earth Sci.*, in press.

Che, Z. C., H. F. Liu, and L. Liu (1994), *The Formation and Evolution of the Central Tianshan Orogenic Belt* (in Chinese), 135 pp., Geol. Publ. House, Beijing.

Chen, Z., and X. Xu (1995), Opening-closing tectonic system at the continental margin of Altay, China, in *Selected Academic Theses of 3rd Symposium of Geology and Mineral Resources of Xinjiang* (in Chinese with English abstract), pp. 15–27, Xinjiang People's Publ. House, Beijing.

Chen, C., H. Lu, D. Jia, D. Cai, and S. Wu (1999), Closing history of the southern Tianshan oceanic basin, western China: An oblique collisional orogeny, *Tectonophysics*, *302*, 23–40, doi:10.1016/S0040-1951(98)00273-X.

Coleman, R. G. (1989), Continental growth of northwest China, *Tectonics*, *8*(3), 621–635, doi:10.1029/TC008i003p00621.

Corrigan, J. (1991), Inversion of apatite fission track data for thermal history information, *J. Geophys. Res.*, *96*(B6), 10,347–10,360, doi:10.1029/91JB00514.

Coutand, I., M. R. Strecker, J. R. Arrowsmith, G. Hilley, R. C. Thiede, A. Korjenkov, and M. Omuraliev (2002), Late Cenozoic tectonic development of the intramontane Alai Valley, (Pamir-Tien Shan region, central Asia): An example of intracontinental deformation due to the India-Asia collision, *Tectonics*, *21*(6), 1053, doi:10.1029/2002TC001358.

DeCelles, P. G., G. E. Gehrels, Y. Najman, A. J. Martin, A. Carter, and E. Garzanti (2004), Detrital geochronology and geochemistry of Cretaceous-early Miocene strata of Nepal: Implications for timing and diachroneity of initial Himalayan Orogenesis, *Earth Planet. Sci. Lett.*, *227*, 313–330, doi:10.1016/j.epsl.2004.08.019.

De Grave, J., and P. Van den haute (2002), Denudation and cooling of the Lake Teletskoye Region in the Altai Mountains (South Siberia) as revealed by apatite fission-track thermochronology, *Tectonophysics*, *349*, 145–159, doi:10.1016/S0040-1951(02)00051-3.

De Grave, J., M. M. Buslov, and P. Van den haute (2004), Intracontinental deformation in Central Asia: Distant effects of India-Eurasia convergence

revealed by apatite fission-track thermochronology, *Himalayan J. Sci.*, *2*, 121–122.

De Grave, J., M. M. Buslov, and P. Van den haute (2007), Distant effects of India-Eurasia convergence and Mesozoic intracontinental deformation in Central Asia: Constraints from apatite fission-track thermochronology, *J. Asian Earth Sci.*, *29*, 188–204, doi:10.1016/j.jseaes.2006.03.001.

De Grave, J., M. M. Buslov, P. Van den haute, J. Metcalf, B. Dehandschutter, and M. O. McWilliams (2009), Multi-method chronometry of the Teletskoye graben and its basement, Siberian Altai Mountains: New insights on its thermo-tectonic evolution, in *Thermochronological Methods: From Paleotemperature Constraints to Landscape Evolution Models*, edited by F. Lisker, B. Ventura, and U. A. Glasmacher, *Geol. Soc. Spec. Publ.*, *324*, 237–259.

de Jong, K., B. Wang, M. Faure, L. S. Shu, D. Cluzel, J. Charvet, G. Ruffet, and Y. Chen (2009), New $^{40}Ar/^{39}Ar$ age constraints on the late Tianshan (Xinjiang, north-western China), with emphasis on Permian fluid ingress, *Int. J. Earth Sci.*, *98*, 1239–1258, doi:10.1007/s00531-008-0338-8.

Delville, N., N. Arnaud, J. M. Ontel, F. Roger, M. Brunel, P. Tapponnier, and E. Sobel (2001), Paleozoic to Cenozoic deformation along the Altyn Tagh Fault in the Altun Shan massif area, Eastern Qilian Shan, NE Tibet, China, in *Paleozoic and Mesozoic Tectonic Evolution of Central Asia: From Continental Assembly to Intracontinental Deformation*, edited by M. S. Hendrix and G. A. Davis, *Mem. Geol. Soc. Am.*, *194*, 269–292, doi:10.1130/0-8137-1194-0.269.

Donelick, R. A. (1991), Crystallographic orientation dependence of mean etchable fission track length in apatite: An empirical model and experimental observation, *Am. Mineral.*, *76*, 83–91.

Donelick, R. A. (1993), A method of fission track analysis utilizing bulk chemical etching of apatite, Patent 6,267,274, U.S. Patent and Trademark Off., Washington, D. C.

Donelick, R. A., R. A. Ketcham, and W. D. Carlson (1999), Variability of apatite fission-track annealing kinetics: II. Crystallographic orientation effects, *Am. Mineral.*, *84*, 1224–1234.

Dumitru, T. A. (1993), A new computer automated microscope stage system for fission track Analysis, *Nucl. Tracks Radiat. Meas.*, *21*, 575–580, doi:10.1016/1359-0189(93)90198-I.

Dumitru, T. A., D. Zhou, E. Z. Chang, and S. A. Graham (2001), Uplift, exhumation, and deformation in the Chinese Tian Shan, in *Paleozoic and Mesozoic Tectonic Evolution of Central Asia: From Continental Assembly to Intracontinental Deformation*, edited by M. S. Hendrix and G. A. Davis, *Mem. Geol. Soc. Am.*, *194*, pp. 71–99, doi:10.1130/0-8137-1194-0.71.

Dunkl, I. (2002), TRACKKEY: A Windows program for calculation and graphical presentation of fission track data, *Comput. Geosci.*, *28*, 3–12, doi:10.1016/S0098-3004(01)00024-3.

Dupont-Nivet, G., W. Krijgsman, C. G. Langereis, H. A. Abels, S. Dai, and X. Fang (2007), Tibetan Plateau aridification linked to global cooling at the Eocene-Oligocene transition, *Nature*, *445*, 635–638, doi:10.1038/nature05516.

Enkin, R., Z. Yang, Y. Chen, and V. Courtillot (1992), Paleomagnetic constraints on the geodynamic history of the major blocks of China from the Permian to the Present, *J. Geophys. Res.*, *97*(B10), 13,953–13,989, doi:10.1029/92JB00648.

Fan, W. M., F. Guo, Y. J. Wang, and G. Lin (2003), Late Mesozoic calc-alkaline volcanism of post-orogenic extension in the northern Da Hinggan Mountains, northeastern China, *J. Volcanol. Geotherm. Res.*, *121*, 115–135, doi:10.1016/S0377-0273(02)00415-8.

Farley, K. A. (2000), Helium diffusion from apatite: General behavior as illustrated by Durango Fluoroapatite, *J. Geophys. Res.*, *105*(B2), 2903–2914, doi:10.1029/1999JB900348.

Farley, K. A., R. Wolf, and L. Silver (1996), The effects of long alpha-stopping distances on (U-Th)/He ages, *Geochim. Cosmochim. Acta*, *60*, 4223–4229, doi:10.1016/S0016-7037(96)00193-7.

Filippova, I. B., V. A. Bush, and A. N. Didenko (2001), Middle Paleozoic subduction belts: The leading factor in the formation of the central Asian fold-and-thrust belt, Russ. *J. Earth Sci.*, *3*, 405–426, doi:10.2205/2001ES000073.

Fu, B., A. Lin, K. Kano, T. Maruyama, and J. Guo (2003), Quaternary folding of the eastern Tian Shan, northwest China, *Tectonophysics*, *369*, 79–101, doi:10.1016/S0040-1951(03)00137-9.

Gaetani, M. (1997), The Karakorum Block in central Asia, from Ordovician to Cretaceous, *Sediment. Geol.*, *109*, 339–359, doi:10.1016/S0037-0738(96)00068-1.

Galbraith, R. F. (2005), *Statistics for Fission Track Analysis*, Chapman and Hall/CRC, Boca Raton, Fla.

Galbraith, R. F., and G. M. Laslett (1993), Statistical models for mixed fission track ages, *Nucl. Tracks Radiat. Meas.*, *21*, 459–470, doi:10.1016/1359-0189(93)90185-C.

Gao, J., M. Li, X. Xiao, Y. Tang, and G. He (1998), Paleozoic tectonic evolution of the Tianshan orogen, northwestern China, *Tectonophysics*, *287*, 213–231, doi:10.1016/S0040-1951(97)00211-4.

Gao, J., L. L. Long, R. Klemd, Q. Qian, D. Y. Liu, X. M. Xiong, W. Su, W. Liu, Y. T. Wang, and F. Q. Yang (2009), Tectonic evolution of the South Tianshan orogen and adjacent regions, NW China: Geochemical and age constraints of granitoid rocks, *Int. J. Earth Sci.*, *98*, 1221–1238, doi:10.1007/s00531-008-0370-8.

Ghose, S., R. J. Mellors, A. M. Korjenkov, M. W. Hamburger, T. L. Pavlis, G. L. Pavlis, M. Omuraliev, E. Mamyrov, and A. R. Muraliev (1997), The M_S = 7.3 1992 Suusamyr, Kyrgyzstan, earthquake in the Tien Shan: 2. Aftershock focal mechanisms and surface deformation, *Bull. Seismol. Soc. Am.*, *87*, 23–38.

Girardeau, J., J. Marcoux, C. J. Allègre, J. P. Bassoullet, Y. Tang, X. Xiao, Y. Zao, and X. Wang (1984), Tectonic environment and geodynamic significance of the Neo-Cimmerian Donqiao ophiolite, Bangong Nu Jiang suture zone, Tibet, China, *Nature*, *307*, 27–31, doi:10.1038/307027a0.

Glorie, S., J. De Grave, M. M. Buslov, M. A. Elburg, D. F. Stockli, A. Gerdes, and P. Van den haute (2010), Multi-method chronometric constraints on the evolution of the northern Kyrgyz Tien Shan batholith (Central Asian Orogenic Belt): From emplacement to exhumation, *J. Asian Earth Sci.*, *38*, 131–146, doi:10.1016/j.jseaes.2009.12.009.

Graham, S. A., D. Zhou, E. Z. Chang, and M. S. Hendrix (1994), Origins of intermontane Jurassic strata of the Chinese Tian Shan, *Geol. Soc. Am. Abstr. Programs*, *26*, A464.

Graham, S. A., M. S. Hendrix, C. L. Johnson, D. Badamgarav, G. Badarch, J. Amory, M. Porte, R. Barsbold, L. E. Webb, and B. R. Hacker (2001), Sedimentary record and tectonic implications of Mesozoic rifting in southern Mongolia, *Geol. Soc. Am. Bull.*, *113*, 1560–1579, doi:10.1130/0016-7606(2001)113<1560:SRATIO>2.0.CO;2.

Green, P. F. (1981), "Track-in-track" length measurements in annealed apatites, *Nucl. Tracks*, *5*, 77–86, doi:10.1016/0191-278X(81)90029-9.

Green, P. F. (1985), A comparison of zeta calibration baselines in zircon, sphene and apatite, *Chem. Geol.*, *58*, 1–22, doi:10.1016/0009-2541(85)90175-5.

Green, P. F., and I. R. Duddy (2006), Interpretation of apatite (U-Th)/He ages and fission track ages from cratons, *Earth Planet. Sci. Lett.*, *244*, 541–547, doi:10.1016/j.epsl.2006.02.024.

Green, P. F., and S. A. Durrani (1978), A quantitative assessment of geometry factors for use in fission track studies, *Nucl. Tracks*, *2*, 207–213.

Green, P. F., I. R. Duddy, A. J. W. Gleadow, and J. F. Lovering (1989), Apatite fission-track analysis as a paleotemperature indicator for hydrocarbon exploration, in *Thermal History of Sedimentary Basins: Methods and Case Histories*, edited by N. D. Naeser and T. H. McCulloch, pp. 181–195, Springer, New York.

Hendrix, M. S. (2000), Evolution of Mesozoic sandstone compositions, southern Junggar, northern Tarim, and western Turpan basins, northwestern China: A detrital record of the ancestral Tian Shan, *J. Sediment. Res.*, *70*, 520–532, doi:10.1306/2DC40924-0E47-11D7-8643000102C1865D.

Hendrix, M., S. A. Graham, A. Carroll, E. Sobel, C. McKnight, B. Schulein, and Z. Wang (1992), Sedimentary record and climatic implications of recurrent deformation in the Tian Shan: Evidence from Mesozoic strata of the north Tarim, south Dzungar, and Turpan basin, northwest China, *Geol. Soc. Am. Bull.*, *104*, 53–79, doi:10.1130/0016-7606(1992)104<0053:SRACIO>2.3.CO;2.

Hendrix, M. S., T. A. Dumitru, and S. A. Graham (1994), Late Oligocene-early Miocene unroofing in the Chinese Tian Shan: An early effect of the India-Asia collision, *Geology*, *22*, 487–490, doi:10.1130/0091-7613(1994)022<0487:LOEMUI>2.3.CO;2.

Heubeck, C. (2001), Assembly of Central Asia during the middle and late Paleozoic, in *Paleozoic and Mesozoic Tectonic Evolution of Central Asia: From Continental Assembly to Intracontinental Deformation*, edited by M. S. Hendrix and G. A. Davis, *Mem. Geol. Soc. Am.*, *194*, 1–22, doi:10.1130/0-8137-1194-0.1.

House, M. A., B. P. Wernicke, K. A. Farley, and T. A. Dumitru (1997), Cenozoic thermal evolution of the central Sierra Nevada, California, from (U-Th)/He thermochronology, *Earth Planet. Sci. Lett.*, *151*, 167–179, doi:10.1016/S0012-821X(97)81846-8.

House, M. A., K. A. Farley, and B. P. Khon (1999), An empirical test of helium diffusion in apatite: Borehole data from the Otway basin, Australia, *Earth Planet. Sci. Lett.*, *170*, 463–474, doi:10.1016/S0012-821X(99)00120-X.

House, M. A., K. A. Farley, and D. Stockli (2000), Helium chronometry of apatite and titanite using Nd-YAG laser heating, *Earth Planet. Sci. Lett.*, *183*, 365–368, doi:10.1016/S0012-821X(00)00286-7.

Hu, A., Z. Zhang, J. Liu, J. Peng, J. Zhang, D. Zhao, S. Yang, and W. Zhou (1986), U-Pb age and evolution of Precambrian metamorphic rocks of the middle Tianshan uplift zone, eastern Tianshan, China, *Geochimica*, *1*, 23–35.

Huang, M., R. Maas, I. S. Buick, and I. S. Williams (2003), Crustal response to continental collisions between the Tibet, Indian, South China and North China blocks: Geochronological constraints from the Songpan-Garze orogenic belt, western China, *J. Metamorph. Geol.*, *21*, 223–240, doi:10.1046/j.1525-1314.2003.00438.x.

Hurford, A. J. (1990), Standardization of fission track dating calibration: Recommendation by the Fission Track Working Group of the I.U.G.S. Subcommission on Geochronology, *Chem. Geol.*, *80*, 171–178.

Hurford, A. J., and P. F. Green (1983), The zeta age calibration of fission-track dating, *Chem. Geol.*, *41*, 285–317, doi:10.1016/S0009-2541(83)80026-6.

Jolivet, M., M. Brunel, D. Seward, Z. Xu, J. Yang, F. Roger, P. Tapponnier, J. Malavieille, N. Arnaud, and C. Wu (2001), Mesozoic and Cenozoic tectonics of the northern edge of the Tibetan Plateau: Fission-track constraints, *Tectonophysics*, *343*, 111–134, doi:10.1016/S0040-1951(01)00196-2.

Jolivet, M., T. J. Dempster, and R. Cox (2003), Répartition de l'U et du Th dans les apatites: Application à la thermochronologie U-Th/He, *C. R. Geosci.*, *335*, 899–906, doi:10.1016/j.crte.2003.08.010.

Jolivet, M., et al. (2007), The Mongolian summits: An uplifted, flat, old but still preserved erosion surface, *Geology*, *35*, 871–874, doi:10.1130/G23758A.1.

Jolivet, M., T. De Boisgrollier, C. Petit, M. Fournier, V. A. Sankov, J.-C. Ringenbach, L. Byzov, A. I. Miroshnichenko, S. N. Kovalenko, and S. V. Anisimova (2009), How old is the Baikal Rift Zone? Insight from apatite fission track thermochro-

nology, *Tectonics*, *28*, TC3008, doi:10.1029/2008TC002404.

Ketcham, R. A. (2005), Forward and inverse modelling of low-temperature thermochronometry data, *Rev. Mineral. Geochem.*, *58*, 275–314, doi:10.2138/rmg.2005.58.11.

Ketcham, R. A., R. A. Donelick, and W. D. Carlson (1999), Variability of apatite fission-track annealing kinetics: III. Extrapolation to geological time scales, *Am. Mineral.*, *84*, 1235–1255.

Ketcham, R. A., R. A. Donelick, and M. B. Donelick (2000), AFTSolve: A program for multikinetic modelling of apatite fission-track data, *Geol. Material Res.*, *2*, 1–32.

Ketcham, R. A., R. A. Donelick, M. L. Balestrieri, and M. Zattin (2009), Reproductibility of apatite fission track length data and thermal history reconstruction, *Earth Planet. Sci. Lett.*, *284*, 504–515, doi:10.1016/j.epsl.2009.05.015.

Khain, V. E. (1985), *Geology of the USSR*, 272 pp., Gebrüder Borntraeger, Berlin.

Khain, E. V., E. E. Bibikova, E. E. Salnikova, A. Kröner, A. S. Gibsher, A. N. Didenko, K. E. Degtyarev, and A. A. Fedotova (2003), The Palaeo-Asian ocean in the Neoproterozoic and early Palaeozoic: New geochronological data and palaeotectonic Reconstructions, *Precambrian Res.*, *122*, 329–358, doi:10.1016/S0301-9268(02)00218-8.

Kirby, E., P. W. Reiners, M. A. Krol, K. X. Whipple, K. V. Hodges, K. A. Farley, W. Tang, and Z. Chen (2002), Late Cenozoic evolution of the eastern margin of the Tibetan Plateau: Inferences from $^{40}Ar/^{39}Ar$ and (U-Th)/He thermochronology, *Tectonics*, *21*(1), 1001, doi:10.1029/2000TC001246.

Konopelko, D., G. Biske, R. Seltmann, O. Eklund, and B. Belyatsky (2007), Hercynian post-collisional A-type granites of the Kokshaal Range, Southern Tien Shan, Kyrgyzstan, *Lithos*, *97*, 140–160, doi:10.1016/j.lithos.2006.12.005.

Kravchinsky, V. A., J.-P. Cogné, W. P. Harbert, and M. I. Kuzmin (2002), Evolution of the Mongol-Okhotsk Ocean as constrained by new palaeomagnetic data from the Mongol-Okhotsk suture zone, Siberia, *Geophys. J. Int.*, *148*, 34–57, doi:10.1046/j.1365-246x.2002.01557.x.

Lai, Q. Z., L. Ding, H. W. Wang, Y. H. Yue, and F. L. Cai (2007), Constraining the stepwise migration of the eastern Tibetan Plateau margin by apatite fission track thermochronology, *Sci. China, Ser, Dokl. Earth Sci.*, *50*, 172–183.

Laurent-Charvet, S. (2001), Accrétions continentales en Asie centro-orientale: Evolution géodynamique et structurale du Tianshan et du Junggar oriental (nord-ouest Chine) au Paléozoïque, thèse de doctorat, 384 pp., Univ. d'Orléans, Orléans, France.

Laurent-Charvet, S., J. Charvet, L. S. Shu, R. S. Ma, and H. F. Lu (2002), Paleozoic late collisional strike-slip deformations in Tianshan and Altay, eastern Xinjiang, NW China, *Terra Nova*, *14*, 249–256, doi:10.1046/j.1365-3121.2002.00417.x.

Laurent-Charvet, S., J. Charvet, P. Monié, and L. S. Shu (2003), Late Paleozoic strike-slip shear zones in eastern Central Asia (NW China): New structural and geochronological data, *Tectonics*, *22*(2), 1009, doi:10.1029/2001TC901047.

Li, Z., W. Song, S. Peng, D. Wang, and Z. Zhang (2004), Mesozoic-Cenozoic tectonic relationships between the Kuqa subbasin and Tian Shan, northwest China: Constraints from depositional records, *Sediment. Geol.*, *172*, 223–249, doi:10.1016/j.sedgeo.2004.09.002.

Lin, W., M. Faure, S. Nomade, Q. Shang, and P. R. Renne (2008), Permian-Triassic amalgamation of Asia: Insights from Northeast China sutures and their place in the final collision of North China and Siberia, *C. R. Geosci.*, *340*, 190–201, doi:10.1016/j.crte.2007.10.008.

Lorencak, M., B. P. Kohn, K. G. Osadetz, and A. J. W. Gleadow (2004), Combined apatite fission track and (U-Th)/He thermochronology in a slowly cooled terrane: Results from a 3440-m-deep drill hole in the southern Canadian Shield, *Earth Planet. Sci. Lett.*, *227*, 87–104, doi:10.1016/j.epsl.2004.08.015.

Lovera, O. M. (1992), Computer program to model $^{40}Ar/^{39}Ar$ diffusion data from multidomain samples, *Comput. Geosci.*, *18*, 789–813, doi:10.1016/0098-3004(92)90025-M.

Lovera, O. M., F. M. Richter, and T. M. Harrison (1989), The $^{40}Ar/^{39}Ar$ thermochronometry for slowly cooled samples having a distribution of diffusion domain sizes, *J. Geophys. Res.*, *94*(B12), 17,917–17,935, doi:10.1029/JB094iB12p17917.

Lovera, O. M., F. M. Richter, and T. M. Harrison (1991), Diffusion domains determined by ^{39}Ar released during step heating, *J. Geophys. Res.*, *96*(B2), 2057–2069, doi:10.1029/90JB02217.

Ma, R. S., C. Y. Wang, and S. F. Ye (1993), Tectonic framework and crustal evolution of Eastern Tianshan mountains, 225 pp., House of Nanjing Univ., Nanjing, China (in Chinese).

Ma, X. (1986), Lithospheric dynamic map of China and adjacent seas with explanatory notes, scale 1/4,000,000, Geol. Publ. House, Beijing.

Matte, P., P. Tapponnier, N. Arnaud, L. Bourjot, J. P. Avouac, P. Vidal, Q. Liu, Y. Pan, and Y. Wang (1996), Tectonics of Western Tibet, between the Tarim and the Indus, *Earth Planet. Sci. Lett.*, *142*, 311–330, doi:10.1016/0012-821X(96)00086-6.

McDougall, I., and T. M. Harrison (1988), *Geochronology and thermochronology by the $^{40}Ar/^{39}Ar$ method*, Oxford Univ. Press, Oxford, U. K.

McDowell, F. W., W. C. McIntosh, and K. A. Farley (2005), A precise ^{40}Ar–^{39}Ar reference age for the Durango apatite (U-Th)/He and fission-track dating standard, *Chem. Geol.*, *214*, 249–263, doi:10.1016/j.chemgeo.2004.10.002.

Mellors, R. J., F. L. Vernon, G. L. Pavlis, G. A. Abers, M. W. Hamburger, S. Ghose, and B. Iliasov (1997), The M_s = 7.3 1992 Suusamyr, Kyrgyzstan, Earthquake: 1. Constraints on Fault Geometry and Source Parameters Based on Aftershocks and Body-Wave Modeling, *Bull. Seismol. Soc. Am.*, *87*, 11–22.

Meng, Q.-R. (2003), What drove late Mesozoic extension of the northern China-Mongolia tract? *Tectonophysics*, *369*, 155–174, doi:10.1016/S0040-1951(03)00195-1.

Metelkin, D. V., I. V. Gordienko, and X. Zhao (2004), Paleomagnetism of Early Cretaceous volcanic rocks from Transbaikalia: Argument for Mesozoic strike-slip motions in Central Asian structure, *Russ. Geol. Geophys.*, *45*, 1404–1417.

Metelkin, D. V., I. V. Gordienko, and V. S. Klimuk (2007), Paleomagnetism of Upper Jurassic basalts from Transbaikalia: New data on the time of closure of the Mongol-Okhotsk Ocean and Mesozoic intraplate tectonics of Central Asia, *Russ. Geol. Geophys.*, *48*, 825–834, doi:10.1016/j.rgg.2007.09.004.

Meyer, B., P. Tapponnier, L. Bourjot, F. Métivier, Y. Gaudemer, G. Peltzer, G. Shunmin, and C. Zhitai (1998), Crustal thickening in Gansu-Qinghai, lithospheric mantle subduction, and oblique, strike-slip controlled growth of the Tibet plateau, *Geophys. J. Int.*, *135*, 1–47, doi:10.1046/j.1365-246X.1998.00567.x.

Murphy, M. A., A. Yin, T. M. Harrison, S. B. Durr, Z. Chen, F. J. Ryerson, W. S. F. Kidd, X. Wang, and X. Zhou (1997), Did the Indo-Asian collision alone create the Tibetan Plateau? *Geology*, *25*, 719–722, doi:10.1130/0091-7613(1997)025<0719:DTIACA>2.3.CO;2.

Najman, Y., and E. Garzanti (2000), Reconstructing early Himalayan tectonic evolution and paleogeography from Tertiary foreland basin sedimentary rocks, northern India, *Geol. Soc. Am. Bull.*, *112*, 435–449, doi:10.1130/0016-7606(2000)112<435:REHTEA>2.0.CO;2.

Persano, C., F. M. Stuart, P. Bishop, and D. N. Barfod (2002), Apatite (U-Th)/He age constraints on the development of the Great Escarpment on the southeastern Australian passive margin, *Earth Planet. Sci. Lett.*, *200*, 79–90, doi:10.1016/S0012-821X(02)00614-3.

Ramstein, G., F. Fluteau, J. Besse, and S. Joussaume (1997), Effect of orogeny, plate motion and land-sea distribution on Eurasian climate change over the past 30 million years, *Nature*, *386*, 788–795, doi:10.1038/386788a0.

Reid, A., C. J. L. Wilson, L. Shun, N. Pearson, and E. Belousova (2007), Mesozoic plutons of the Yidun arc, SW China: U/Pb geochronology and Hf isotopic signature, *Ore Geol. Rev.*, *31*, 88–106, doi:10.1016/j.oregeorev.2004.11.003.

Reiners, P. W., R. Brady, K. A. Farley, J. E. Fryxell, B. Wernicke, and D. Lux (2000), Helium and argon thermochronometry of the Gold Butte block, south Virgin Mountains, Nevada, *Earth Planet. Sci. Lett.*, *178*, 315–326, doi:10.1016/S0012-821X(00)00080-7.

Reiners, P. W., T. L. Spell, S. Nicolescu, and K. A. Zanetti (2004), Zircon (U-Th)/He thermochronometry: He diffusion and comparison with $^{40}Ar/^{39}Ar$ dating, *Geochim. Cosmochim. Acta*, *68*, 1857–1887, doi:10.1016/j.gca.2003.10.021.

Ren, J., K. Tamaki, S. Li, and Z. Junxia (2002), Late Mesozoic and Cenozoic rifting and its dynamic setting in Eastern China and adjacent areas, *Tectonophysics*, *344*, 175–205, doi:10.1016/S0040-1951(01)00271-2.

Ritts, B. D., and U. Biffi (2001), Mesozoic northeast Qaidam basin: Response to contractional reactivation of the Qilian Shan, and implications for the extent of Mesozoic intracontinental deformation in central Asia, in *Paleozoic and Mesozoic Tectonic Evolution of Central Asia: From Continental Assembly to Intracontinental Deformation*, edited by M. S. Hendrix and G. A. Davis, *Mem. Geol. Soc. Am.*, *194*, 293–316, doi:10.1130/0-8137-1194-0.293.

Roger, F., J. Malavieille, P. H. Leloup, S. Calassou, and Z. Xu (2004), Timing of granite emplacement and cooling in the Songpan-Garzê fold belt (eastern Tibetan Plateau) with tectonic implications, *J. Asian Earth Sci.*, *22*, 465–481, doi:10.1016/S1367-9120(03)00089-0.

Roger, F., M. Jolivet, and J. Malavieille (2008), Tectonic evolution of the Triassic fold belts of Tibet, *C. R. Geosci.*, *340*, 180–189.

Roger, F., M. Jolivet, R. Cattin, and J. Malavieille (2010), Mesozoic-Cenozoic tectonothermal evolution of the eastern part of the Tibetan Plateau (Songpan-Garzê, Longmen Shan area): Insights from thermochronological data and simple thermal modeling, *Geol. Soc. Spec. Publ.*, *353*, in press.

Rowley, D. B. (1996), Age of initiation of collision between India and Asia: A review of stratigraphic data, *Earth Planet. Sci. Lett.*, *145*, 1–13, doi:10.1016/S0012-821X(96)00201-4.

Searle, M. P. (1991), *Geology and Tectonics of the Karakorum Mountains*, 358 pp., John Wiley, New York.

Şengör, A. C., and B. A. Natal'in (1996), Turkic-type orogeny and its role in the making of continental crust, *Annu. Rev. Earth Planet. Sci.*, *24*, 263–337, doi:10.1146/annurev.earth.24.1.263.

Şengör, A. M. C., B. A. Natal'in, and V. S. Burtman (1993), Evolution of the Altaïd tectonic collage and Paleozoic crustal growth in Eurasia, *Nature*, *364*, 299–307, doi:10.1038/364299a0.

Seward, D., R. Spikings, G. Viola, A. Kounov, G. M. H. Ruiz, and N. Naeser (2000), Etch times and operator variation for spontaneous track lengths measurements in apatites: An intra-laboratory check, *OnTrack*, *10*, 16–21.

Shao, J., B. Mu, and L. Zhang (2000), Deep geological process and its shallow response during Mesozoic transfer of tectonic framework in eastern north China, *Geol. Rev.*, *46*, 32–40.

Shu, L. S., J. Charvet, L. Z. Guo, H. F. Lu, and S. Laurent-Charvet (1999), A large-scale dextral ductile strike-slip zone: The Aqqikkudug-Weiya zone along the northern margin of the Central Tianshan belt, Xinjiang, NW China, *Dizhi Xuebao*, *73*, 148–162.

Shuster, D. L., R. M. Flowers, and K. A. Farley (2006), The influence of natural radiation damage on

helium diffusion kinetics in apatite, *Earth Planet. Sci. Lett.*, doi:10.1016/j.epsl.2006.07.028.

Sobel, E. R. (1995), Basin analysis and apatite thermochronology of the Jurassic-Paleogene Western Tarim basin, Ph.D. dissertation, 308 pp., Stanford Univ., Stanford, Calif.

Sobel, E. R. (1999), Basin analysis of the Jurassic-Lower Cretaceous southwest Tarim basin, northwest China, *Geol. Soc. Am. Bull.*, *111*, 709–724, doi:10.1130/0016-7606(1999)111<0709:BAOTJL>2.3.CO;2.

Sobel, E. R., and N. Arnaud (1996), Age controls on origin and cooling of the Altyn Tagh range, NW China, *Geol. Soc. Am. Abstr. Programs*, *28*, A67.

Sobel, E. R., and N. Arnaud (1999), A possible middle Paleozoic suture in the Altyn Tagh, NW China, *Tectonics*, *18*(1), 64–74, doi:10.1029/1998TC900023.

Sobel, E. R., and T. A. Dumitru (1997), Thrusting and exhumation around the margins of the western Tarim basin during the India-Asia collision, *J. Geophys. Res.*, *102*(B3), 5043–5063, doi:10.1029/96JB03267.

Sobel, E. R., and D. Seward (2010), Influence of etching conditions on apatite fission-track etch pit diameter, *Chem. Geol.*, *271*, 59–69, doi:10.1016/j.chemgeo.2009.12.012.

Sobel, E. R., M. Oskin, D. Burbank, and A. Mikolaichuk (2006), Exhumation of basement-cored uplifts: Example of the Kyrgyz Range quantified with apatite fission track thermochronology, *Tectonics*, *25*, TC2008, doi:10.1029/2005TC001809.

Söderlund, P., J. Juez-Larre, L. M. Page, and T. J. Dunai (2005), Extending the time range of (U-Th)/He thermochronometry in slowly cooled terranes: Paleozoic to Cenozoic exhumation history of southeast Sweden, *Earth Planet. Sci. Lett.*, *239*, 266–275, doi:10.1016/j.epsl.2005.09.009.

Tagami, T. (1987), Determination of zeta calibration constant for fission track dating, *Nucl. Tracks Radiat. Meas.*, *13*, 127–130, doi:10.1016/1359-0189(87)90023-9.

Tang, F., Z. X. Luo, Z. H. Zhou, H. L. You, J. A. Georgi, Z. L. Tang, and X. Z. Wang (2001), Biostratigraphy and Cimmerian environment of the dinosaur-bearing sediments in Lower Cretaceous of Mazongshan area, Gansu Province, China, *Cretaceous Res.*, *22*, 115–129, doi:10.1006/cres.2000.0242.

Tapponnier, P., M. Mattaeur, F. Proust, and C. Cassaigneau (1981), Mesozoic ophiolites, sutures, and large-scale tectonic movements in Afghanistan, *Earth Planet. Sci. Lett.*, *52*, 355–371, doi:10.1016/0012-821X(81)90189-8.

Tapponnier, P., G. Peltzer, and R. Armijo (1986), On the mechanics of the collision between India and Asia, in *Collision Tectonics*, edited by M. P. Coward and A. C. Ries, *Geol. Soc. Spec. Publ*, *19*, 115–157.

Vassallo, R., M. Jolivet, J.-F. Ritz, R. Braucher, C. Larroque, C. Sue, M. Todbileg, and D. Javkhlanbold (2007), Uplift age and rates of the Gurvan Bogd system (Gobi-Altay) by apatite fission track analysis, *Earth Planet. Sci. Lett.*, *259*, 333–346, doi:10.1016/j.epsl.2007.04.047.

Vincent, S. J., and M. B. Allen (1999), Evolution of the Minle and Chaoshui Basins, China: Implications for Mesozoic strike-slip basin formation in Central Asia, *Geol. Soc. Am. Bull.*, *111*, 725–742, doi:10.1130/0016-7606(1999)111<0725:EOTMAC>2.3.CO;2.

Vincent, S. J., and M. B. Allen (2001), Sedimentary record of Mesozoic intracontinental deformation in the eastern Junggar Basin, north–west China: Response to orogeny at the Asian margin, in *Palaeozoic and Mesozoic Tectonic Evolution of Central and Eastern Asia: From Continental Assembly to Intracontinental Deformation*, edited by M. S. Hendrix and G. A. Davis, *Mem. Geol. Soc. Am.*, *194*, 341–360, doi:10.1130/0-8137-1194-0.341.

Wang, B., Z. Lang, X. Li, X. Qu, T. Li, C. Huang, and X. Cui (1994), *Comprehensive Survey Of Geological Sections in the West Tianshan of Xinjiang, China*, 202 pp., Sci. Publ. House, Beijing.

Wang, B., D. Cluzel, L. S. Shu, M. Faure, J. Charvet, Y. Chen, S. Meffre, and K. de Jong (2009), Evolution of calc-alkaline to alkaline magmatism through Carboniferous convergence to Permian transcurrent tectonics, western Chinese Tianshan, *Int. J. Earth Sci.*, *98*, 1275–1298, doi:10.1007/s00531-008-0408-y.

Wang, B., M. Faure, L. Shu, K. de Jong, J. Charvet, D. Cluzel, B. Jahn, Y. Chen, and G. Ruffet (2010), Structural and geochronological study of high-pressure metamorphic rocks in the Kekesu section (northwestern China): Implications for the late Paleozoic tectonics of the Southern Tianshan, *J. Geol.*, *118*, 59–77, doi:10.1086/648531.

Wang, F., X. H. Zhou, L. C. Zhang, J. F. Ying, Y. T. Zhang, F. Y. Wu, and R. X. Zhu (2006), Late Mesozoic volcanism in the Great Xing'an Range (NE China): Timing and implications for the dynamic setting of NE Asia, *Earth Planet. Sci. Lett.*, *251*, 179–198, doi:10.1016/j.epsl.2006.09.007.

Wang, J., Y. J. Wang, Z. C. Liu, J. Q. Li, and P. Xi (1999), Cenozoic environmental evolution of the Qaidam Basin and its implications for the uplift of the Tibetan Plateau and the drying of central Asia, *Palaeogeogr. Palaeoclimatol. Palaeoecol.*, *152*, 37–47, doi:10.1016/S0031-0182(99)00038-3.

Wang, Z., J. Wu, X. Lu, and C. Liu (1990), *Polycyclic Tectonic Evolution and Metallogeny of the Tianshan Mountains*, 217 pp., Sci. Press, Beijing.

Warnock, A. C., P. K. Zeitler, R. A. Wolf, and S. C. Bergman (1997), An evaluation of low-temperature apatite U-Th/He thermochronology, *Geochim. Cosmochim. Acta*, *61*, 5371–5377, doi:10.1016/S0016-7037(97)00302-5.

Wartes, M. A., A. R. Carroll, and T. J. Greene (2002), Permian sedimentary record of the Turpan-Hami basin and adjacent regions, northwest China: Constraints on postamalgamation tectonic evolution, *Geol. Soc. Am. Bull.*, *114*, 131–152, doi:10.1130/0016-7606(2002)114<0131:PSROTT>2.0.CO;2.

Watson, M. P., A. B. Hayward, D. N. Parkinson, and Z. M. Zhang (1987), Plate tectonic history, basin development and petroleum source rock deposition onshore China, *Mar. Pet. Geol.*, *4*, 205–225, doi:10.1016/0264-8172(87)90045-6.

Webb, L. E., S. A. Graham, C. L. Johnson, G. Badarch, and M. S. Hendrix (1999), Occurrence, age and implications of the Yagan-Onch Hayrhan metamorphic core complex, southern Mongolia, *Geology*, *27*, 143, doi:10.1130/0091-7613(1999)027<0143:OAAIOT>2.3.CO;2.

Windley, B. F., M. B. Allen, C. Zhang, Z. Y. Zhao, and G. R. Wang (1990), Paleozoic accretion and Cenozoic redeformation of the Chinese Tien Shan range, central Asia, *Geology*, *18*, 128–131, doi:10.1130/0091-7613(1990)018<0128:PAACRO>2.3.CO;2.

Windley, B. F., D. Alexeiev, W. Xiao, A. Kröner, and G. Badarch (2007), Tectonic models for accretion of the Central Asian Orogenic Belt, *J. Geol. Soc.*, *164*, 31–47, doi:10.1144/0016-76492006-022.

Wolf, R., K. Farley, and D. Kass (1998), Modelling of the temperature sensitivity of the apatite (U-Th)/He thermochronometer, *Chem. Geol.*, *148*, 105–114, doi:10.1016/S0009-2541(98)00024-2.

Xinjiang Bureau of Geology and Mineral Resources (XBGMR) (1969), Geological maps of the Bayanbulak area, scale 1:200,000, Geol. Publ. House, Beijing.

Xinjiang Bureau of Geology and Mineral Resources (XBGMR) (1971), Geological maps of the western Bayanbulak area, scale 1:200,000, Geol. Publ. House, Beijing.

Xinjiang Bureau of Geology and Mineral Resources (XBGMR) (1973), Geological maps of the eastern Yili area, scale 1:200,000, Geol. Publ. House, Beijing.

Xu, G., and P. J. J. Kamp (2000), Tectonics and denudation adjacent to the Xianshuihe Fault, eastern Tibetan Plateau: Constraints from fission track thermochronology, *J. Geophys. Res.*, *105*(B8), 19,231–19,251, doi:10.1029/2000JB900159.

Yin, A. (2006), Cenozoic tectonic evolution of the Himalayan orogen as constrained by along-strike variation of structural geometry, exhumation history, and foreland sedimentation, *Earth Sci. Rev.*, *76*, 1–131, doi:10.1016/j.earscirev.2005.05.004.

Yin, A. (2010), Cenozoic tectonic evolution of Asia: A preliminary synthesis, *Tectonophysics*, *488*, 293–325, doi:10.1016/j.tecto.2009.06.002.

Yin, A., S. Nie, P. Craig, T. M. Harrison, F. J. Ryerson, Q. Xianglin, and Y. Geng (1998), Late Cenozoic tectonic evolution of the southern Chinese Tian Shan, *Tectonics*, *17*(1), 1–27, doi:10.1029/97TC03140.

Yuan, W., A. Carter, J. Dong, Z. Bao, Y. An, and Z. Guo (2006), Mesozoic-Tertiary exhumation history of the Altai Mountains, northern Xinjiang, China: Constraints from apatite fission track data, *Tectonophysics*, *412*, 183–193, doi:10.1016/j.tecto.2005.09.007.

Zhou, D., S. A. Graham, E. Z. Chang, B. Wang, and B. Hacker (2001), Paleozoic tectonic amalgamation of the Chinese Tian Shan: Evidence from a transect along the Dushanzi-Kuqa Highway, in *Paleozoic and Mesozoic Tectonic Evolution of Central and Eastern Asia: From Continental Assembly to Intracontinental Deformation*, edited by M. S. Hendrix and G. A. Davis, *Mem. Geol. Soc. Am.*, *194*, 71–99.

Zhou, M. F., D. P. Yan, P. M. Vasconcelos, J. W. Li, and R. Z. Hu (2008), Structural and geochronological constraints on the tectono-thermal evolution of the Danba domal terrane, eastern margin of the Tibetan Plateau, *J. Asian Earth Sci.*, *33*, 414–427, doi:10.1016/j.jseaes.2008.03.003.

Ziegler, J. F. (1977), *Helium: Stopping Powers and Ranges in All Elemental Matter*, 367 pp., Pergamon, New York.

Zorin, Y. A. (1999), Geodynamics of the western part of the Mongolia-Okhotsk collisional belt, Trans-Baikal region (Russia) and Mongolia, *Tectonophysics*, *306*, 33–56, doi:10.1016/S0040-1951(99)00042-6.

Zorin, Y. A., V. V. Mordvinova, E. K. Turutanov, B. G. Belichenko, A. A. Artemyev, G. L. Kosarev, and S. S. Gao (2002), Low seismic velocity layers in the Earth's crust beneath Eastern Siberia (Russia) and Central Mongolia: Receiver function data and their possible geological implication, *Tectonophysics*, *359*, 307–327, doi:10.1016/S0040-1951(02)00531-0.

J. Charreau, Centre de Recherches Pétrographiques et Géochimiques, Vandoeuvre lès Nancy, France. (charreau@crpg.cnrs-nancy.fr)

Y. Chen, Université d'Orléans, Institut des Sciences de la Terre d'Orléans, Orléans, France. (Yan.Chen@univ-orleans.fr)

S. Dominguez, Université Montpellier 2, Laboratoire Géosciences Montpellier, UMR 5243 CNRS/INSU, Montpellier, France. (dominguez@gm.univ-montp2.fr)

M. Jolivet, Université Rennes 1, Laboratoire Géosciences Rennes, UMR 6118 CNRS/INSU, Rennes, France. (marc.jolivet@univ-rennes1.fr)

Y. Li, Institute of Geology and Mineral Resources, Urumqi, China.

Q. Wang, State Key Laboratory of Lithospheric Evolution, Institute of Geology and Geophysics, Chinese Academy of Sciences, Beijing, China. (qcwang@mail.iggcas.ac.cn)